Design, synthesis and pharmacological evaluation of N-benzyl-piperidinyl-aryl-acylhydrazone derivatives as donepezil hybrids: Discovery of novel multi-target anti-alzheimer prototype drug candidates

Accepted Manuscript

Design, synthesis and pharmacological evaluation of *N*-benzyl-piperidinyl-aryl-acylhydrazone derivatives as donepezil hybrids: Discovery of novel multi-target anti-alzheimer prototype drug candidates

Flávia Pereira Dias Viegas, Matheus de Freitas Silva, Miguel Divino da Rocha, Maísa Rosa Castelli, Mariana Máximo Riquiel, Rafael Pereira Machado, Sarah Macedo Vaz, Laís Medeiros Simões de Lima, Karla Cristine Mancini, Patrícia Cruz Marques de Oliveira, Élida Parreira Morais, Vanessa Silva Gontijo, Fernanda Motta R. da Silva, Dora D'Alincourt da Fonseca Peçanha, Newton Gonçalves Castro, Gilda A. Neves, Alexandre Giusti-Paiva, Fabiana Cardoso Vilela, Lidiane Orlandi, Ihosvany Camps, Márcia Paranho Veloso, Luis Felipe Leomil Coelho, Marisa Ionta, Guilherme Álvaro Ferreira-Silva, Rodrigo Machado Pereira, Laurent E. Dardenne, Isabella Alvim Guedes, Wellerson de Oliveira Carneiro Junior, Paula Maria Quaglio Bellozi, Antônio Carlos Pinheiro de Oliveira, Fábio Furlan Ferreira, Letizia Pruccoli, Andrea Tarozzi, Claudio Viegas, Jr.

PII: S0223-5234(18)30079-5

DOI: 10.1016/j.ejmech.2018.01.066

Reference: EJMECH 10143

To appear in: *European Journal of Medicinal Chemistry*

Received Date: 12 December 2017

Revised Date: 18 January 2018

Accepted Date: 19 January 2018

Design, Synthesis and Pharmacological Evaluation of *N*-Benzyl-Piperidinyl-Aryl-Acyl-hydrazone Derivatives as Donepezil Hybrids: Discovery of Novel Multi-Target Anti-Alzheimer Prototype Drug Candidates

Flávia Pereira Dias Viegas[1], Matheus de Freitas Silva[1], Miguel Divino da Rocha[1], Maísa Rosa Castelli[1], Mariana Máximo Riquiel[1], Rafael Pereira Machado[1], Sarah Macedo Vaz[1], Laís Medeiros Simões de Lima[1], Karla Cristine Mancini[1], Patrícia Cruz Marques de Oliveira[1], Élida Parreira Morais[1], Vanessa Silva Gontijo[1], Fernanda Motta R. da Silva[2], Dora D'Alincourt da Fonseca Peçanha[2], Newton Gonçalves Castro[2], Gilda A. Neves[2], Alexandre Giusti-Paiva[4], Fabiana Cardoso Vilela[4], Lidiane Orlandi[4], Ihosvany Camps[5], Márcia Paranho Veloso[6], Luis Felipe Leomil Coelho[7], Marisa Ionta[4], Guilherme Álvaro Ferreira-Silva[4], Rodrigo Machado Pereira[4], Laurent E. Dardenne[8], Isabella Alvim Guedes[8], Wellerson de Oliveira Carneiro Junior[9], Paula Maria Quaglio Bellozi[9], Antônio Carlos Pinheiro de Oliveira[9], Fábio Furlan Ferreira[10], Letizia Pruccoli[11], Andrea Tarozzi[11] and Claudio Viegas Jr.[1]*

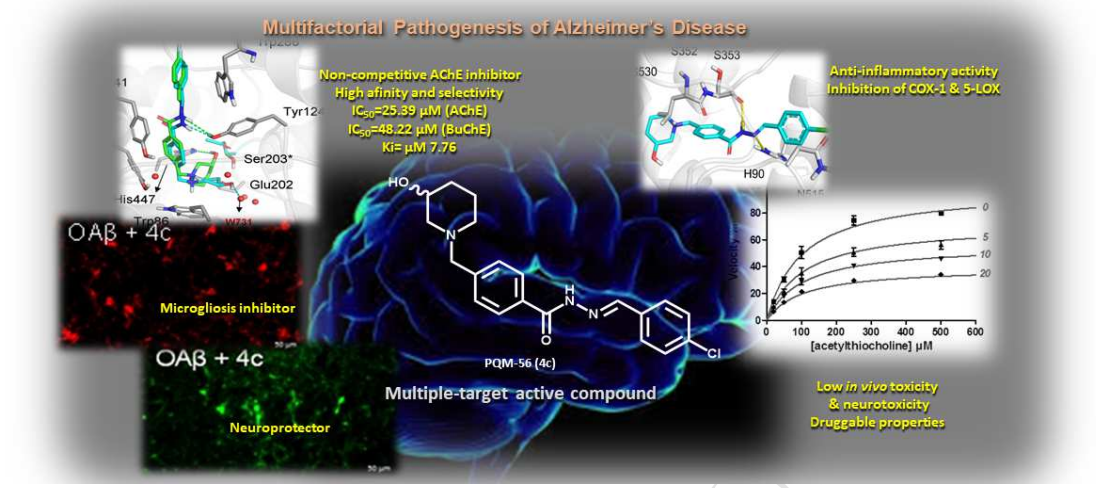

Design, Synthesis and Pharmacological Evaluation of *N*-Benzyl-Piperidinyl-Aryl-Acylhydrazone Derivatives as Donepezil Hybrids: Discovery of Novel Multi-Target Anti-Alzheimer Prototype Drug Candidates

*Flávia Pereira Dias Viegas[1], Matheus de Freitas Silva[1], Miguel Divino da Rocha[1], Maísa Rosa Castelli[1], Mariana Máximo Riquiel[1], Rafael Pereira Machado[1], Sarah Macedo Vaz[1], Laís Medeiros Simões de Lima[1], Karla Cristine Mancini[1], Patrícia Cruz Marques de Oliveira[1], Élida Parreira Morais[1], Vanessa Silva Gontijo[1], Fernanda Motta R. da Silva[2], Dora D'Alincourt da Fonseca Peçanha[2], Newton Gonçalves Castro[2], Gilda A. Neves[2], Alexandre Giusti-Paiva[4], Fabiana Cardoso Vilela[4], Lidiane Orlandi[4], Ihosvany Camps[5], Márcia Paranho Veloso[6], Luis Felipe Leomil Coelho[7], Marisa Ionta[4], Guilherme Álvaro Ferreira-Silva[4], Rodrigo Machado Pereira[4], Laurent E. Dardenne[8], Isabella Alvim Guedes[8], Wellerson de Oliveira Carneiro Junior[9], Paula Maria Quaglio Bellozi[9], Antônio Carlos Pinheiro de Oliveira[9], Fábio Furlan Ferreira[10], Letizia Pruccoli[11], Andrea Tarozzi[11] and Claudio Viegas Jr.[1]**

[1] Institute of Chemistry, Laboratory of Research on Medicinal Chemistry, Federal University of Alfenas, MG, Brazil, 37133-840

[2] Laboratory of Molecular Pharmacology, Institute of Biomedical Sciences, Federal University of Rio de Janeiro, RJ, 21941-902, Brazil.

[3] Institute of National Sciences, Federal University of Alfenas, MG, 37130-000, Brazil

[4] Institute of Biomedical Sciences, Federal University of Minas Gerais, MG, 37130-000, Brazil

[5] Institute of Exact Sciences, Federal University of Alfenas, MG, 37130-000, Brazil

[6] Faculty of Pharmacy, Federal University of Alfenas, MG, 37130-000, Brazil

[7] Laboratory of Vaccines, Institute of Biomedical Sciences, Federal University of Alfenas, MG, 37130-000, Brazil.

[8]National Laboratory of Computational Sciences, Petrópolis, RJ, 25651-075, Brazil

[9]Institute of Biological Sciences, Federal University of Minas Gerais, MG, 31270-901, Brazil

[10]Centre of Natural and Human Sciences, Federal University of ABC, Santo André, SP, 09210-580, Brazil

[11]Department for Life Quality Studies, Alma Mater Studiorum-University of Bologna, Rimini, 47921, Italy

*Corresponding author: Claudio Viegas Jr., Institute of Chemistry, Laboratory of Research on Medicinal Chemistry, Avenida Jovino Fernandes Sales, 2600. Federal University of Alfenas. 37130.000 Alfenas-MG, Brazil. Tel +55 (35) 3701-1880. e-mail: cvjviegas@gmail.com

ABSTRACT

A new series of sixteen multifunctional *N*-benzyl-piperidine-aryl-acylhydrazones hybrid derivatives was synthesized and evaluated for multi-target activities related to Alzheimer's disease (AD). The molecular hybridization approach was based on the combination, in a single molecule, of the pharmacophoric *N*-benzyl-piperidine subunit of donepezil, the substituted hydroxy-piperidine fragment of the AChE inhibitor LASSBio-767, and an acylhydrazone linker, a privileged structure present in a number of synthetic aryl- and aryl-acylhydrazone derivatives with significant AChE and anti-inflammatory activities. Among them, compounds **4c**, **4d**, **4g** and **4j** presented the best AChE inhibitory activities, but only compounds **4c** and **4g** exhibited concurrent anti-inflammatory activity *in vitro* and *in vivo*, against amyloid beta oligomer (AβO) induced neuroinflammation. Compound **4c** also showed the best *in vitro* and *in vivo* neuroprotective effects against AβO-induced neurodegeneration. In addition, compound **4c** showed a similar binding mode to donepezil in both acetylated and free forms of AChE enzyme in molecular docking studies and did not show relevant toxic effects on *in vitro* and *in vivo* assays, with good predicted ADME parameters *in silico*. Overall, all these results highlighted compound **4c** as a promising and innovative multi-target drug prototype candidate for AD treatment.

Keywords: Alzheimer's disease, multi-target directed ligands, *N*-benzyl-piperidine derivatives, donepezil analogs, acetylcholinesterase inhibition, anti-inflammatory activity, COX inhibition, amyloid beta oligomers, neuroprotection.

1. Introduction

Alzheimer's disease (AD) is a severe degenerative disorder of the central nervous system (CNS) and is the most common type of dementia among the population above age 65. AD is characterized by progressive loss in cognition, decrease in motor and functional capacity, impairment in behavioral and social autonomy and death.[1–5] Pharmacotherapy of AD is only palliative and restricted to a few available drugs that act either through the inhibition of acetylcholinesterase (AChE) enzyme or through a mild neuroprotective effect, alleviating the symptoms and slightly delaying the progress of the disease. AD is characterized by multiple physiological and biochemical disturbances involving concurrently operating chemical mediators and numerous protein targets.[1,6–9] During the last years, we have observed huge advances in the understanding of the complex multi factorial pathophysiology of AD. Although its etiology is not completely understood, it is well established that concomitant and interconnected multiple factors are decisive for the onset, progression and severity of AD. It is well accepted that an idiopathic physiological deregulation in some brain regions (e.g. hippocampus and cortex) is responsible for an overproduction of Aβ-peptide (Aβ), cleaved from its precursor protein by β- and γ-secretases. Aβ-fragments may form neurotoxic soluble oligomers (AβO) and, in turn, insoluble fibrillar aggregates or senile plaques. Associated with amyloid neuropathology, hyperphosphorylation of neuronal microtubule constitutive τ-protein occurs and leads to a collapse in the structure of microtubules, disruption of axonal transport, and accumulation of intracellular neurofibrillary tangles.[10–15] Acting together, these two biochemical factors lead to cumulative changes in CNS homeostasis and function, eventually leading to neuronal death.[9,13]

Several studies also suggest that Aβ deposits and neurofibrillary tangles provide stimuli for neuroinflammation, which contribute to significantly exacerbate the AD pathogenic processes.[16,17] Among the brain cells, the activated microglia cells have been shown to be involved in the secretion of pro-inflammatory cytokines, such as interleukin-1 (IL-1β), IL-6 and tumor necrosis factor alpha (TNF-α), thereby contributing towards the progress of AD.[18,19] Further, studies on AD pathogenesis have demonstrated that microglia produce Aβ, which is in itself pro-inflammatory and causes activation of several

inflammatory componentes.[20] The pro-inflammatory cytokines act as potent stimuli in brain inflammation through upregulation of cytosolic PLA2 and cyclooxygenase-1 (COX-1) and -2 (COX-2).[21] Upon inflammatory stimuli, COX-1, being constitutive in microglia, is responsible for the primary inflammatory response by inducing the production of prostaglandin, mainly prostaglandin E2. By contrast, COX-2 expression in neurons is responsible, upon its induction, for a later and secondary inflammatory response.[21] Therefore, drugs designed to treat the different neuroinflammatory conditions mediated by COX-1 and COX-2 are needed.

Thus, in addition to cholinergic signaling, excitotoxic mechanisms and the amyloid cascade, microglial cells and neuroinflammation have emerged as essential targets in the polypharmacology-derived concept of multi-target directed drugs for AD, representing a new paradigm in their design and discovery.[1,2,22–28]

Donepezil (**1**) is a potent AChE inhibitor with an IC_{50} of 5.7 nM and a 1250-fold higher selectivity over butyrylcholinesterase (BuChE) and a long duration effect. To date, donepezil is the reference drug for mild and moderate AD treatment and, in some cases, is recommended to be used in association with the anti-excitotoxic drug memantine for the most severe cases of the disease.[25,29–33]

In the search for novel bioactive chemical entities, the *N*-acylhydrazone moiety deserves highlight as a privileged structure, capable to act as pharmacophore or auxophore subunit in different pharmaceutic classes, with a variety of action profile, depending on the other functionalities present in the molecular structure.[34,35] Recently, *Silva* and co-workers synthetized a series of *N*-acylhydrazones, designed as AChE inhibitors. The pharmacological evaluation evidenced that these derivatives showed significant AChE inhibitory activity. *Turnaturi* and co-workers have also observed the antioxidant capacity of some *N*-acylhydrazones with metal chelant ability[36,37]. As a part of an ongoing project that aims at the discovery of innovative multi-target directed drugs, we describe herein the discovery of novel donepezil-derived *N*-acyl-aryl-hydrazone ligands with multifunctional profile as promising drug candidates for the treatment of AD. The design of the target-molecules was based on molecular hybridization of the pharmacophoric subunit *N*-benzyl-piperidine core (Fig. 1, a) present in structure of donepezil (**1**), with a common 3-*O*-substituted-piperidine subunit (b) present in the structure of the AChE inhibitor LASSBio-

767 (**2**), and the insertion of a *N*-acyl-arylhydrazone functionality (c, d) considered a privileged structure present in a number of anti-inflammatory [35,38–42], AChE inhibitors and antioxidant drug prototypes in the literature [36,37]. Our aim was to generate a novel chemical library (Fig. 1), with an innovative scaffold to explore structure-activity relationship of ligand candidates with a multitarget profile, that could act as AChE inhibitors, anti-neuroinflammatory and neuroprotectants.

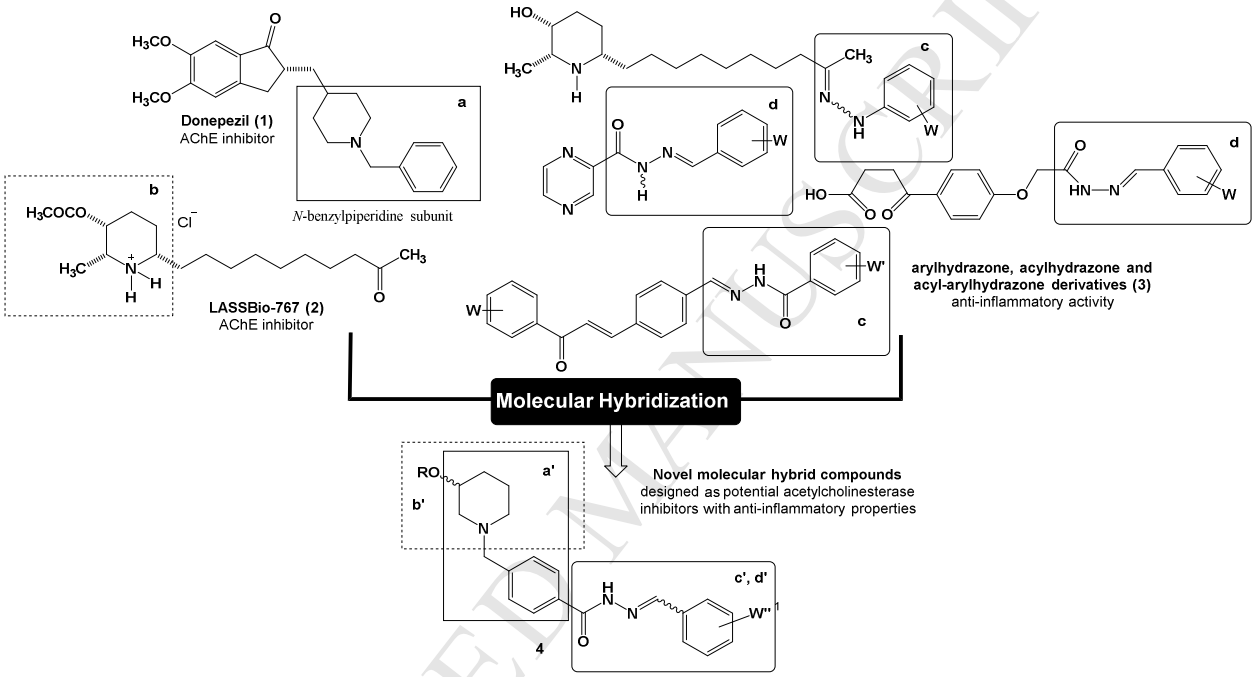

Fig. 1. Design of a new series (**4**) of multi-target directed ligands (MTDLs) based on the molecular hybridization of the structures of donepezil (**1**), the AChE inhibitor LASSBio-767 (**2**) and a series of anti-inflammatory *N*-aryl-acylhydrazone derivatives (**3**).

2. Results and discussion

2.1. Chemistry

4-carboxybenzaldehyde (**5**) and *rac*-3-hydroxypiperidine (**7**) were used as starting materials to prepare the key intermediate 4-((3-hydroxypiperidin-1-yl)-methyl)-benzohydrazide **9** according to the synthetic approaches described in Scheme 1 (experimental details in the supporting information material). Initially, 4-carboxybenzadehyde was reacted with $SOCl_2$/DMF, followed by treatment with anhydrous MeOH to provide the ester derivative **6**. Reductive amination reaction between ester **6** and

rac-3-hydroxypiperidine (**7**) in the presence of $ZnCl_2/NaBH_3CN$ led to the desired 3-hydroxy-*N*-benzyl-piperidine ester **8** that was then converted to the key intermediate *N*-acylhydrazone **9**. In a final step, coupling reactions of **9** and the benzaldehydes **10a-l** led to the target molecules **4a-l** in good yields. Additional 3-*O*-acetyl-piperidine derivatives **4m, 4n** and **4o** were prepared directly by reaction of Ac_2O/4-DMAP with the correspondent 3-hydroxy precursor. Compound **4h** were obtained by catalytic hydrogenation of the *para*-NO_2 derivative **4d** in quantitative yields. Compound **4n** were obtained by reaction of Ac_2O/4-DMAP and catalytic hydrogenation of the *para*-NO_2 with **4d**.

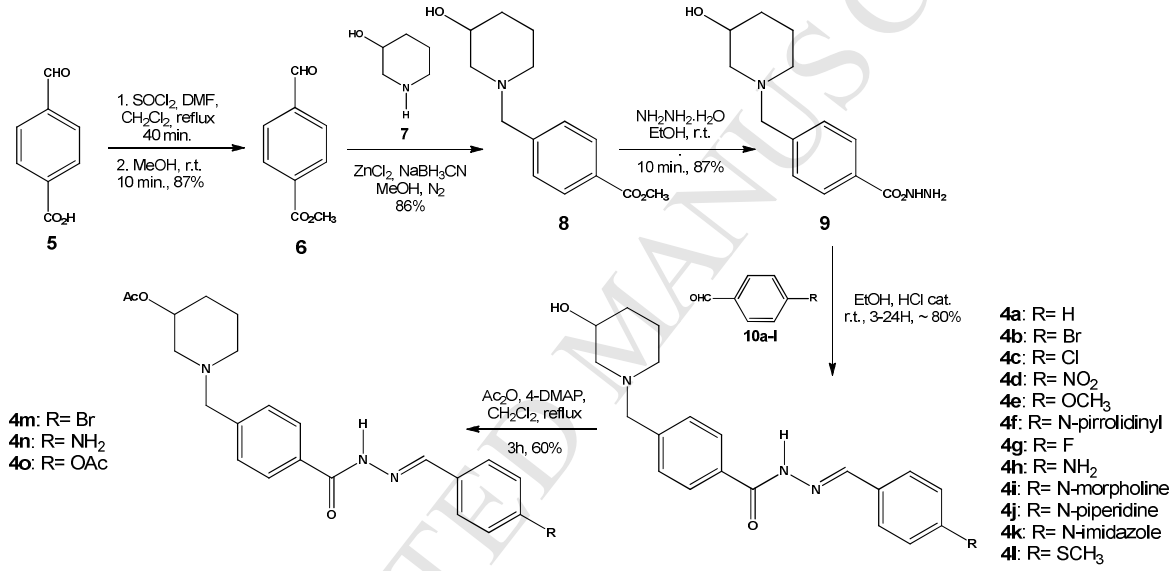

Scheme 1. Synthetic route for the target-compounds **4a-o**

The purity of all compounds was determined as 94-98% by UPLC-UV. Considering that the starting material was the racemic 3-hydroxypiperidine, the products were also racemic, but the NMR and MS analysis of all compounds did not indicate the formation of diastereoisomers. [34,43] We suppose that the coupling reaction between the hydrazide **9** and the functionalized benzaldehydes furnished only the most stable *E* relative configuration at the hydrazone moiety. In order to verify this, the compounds were subjected to X-ray powder diffraction analysis that confirmed the *E* relative configuration, as can be seen in Fig. 2 for compounds **4c** and **4g**.

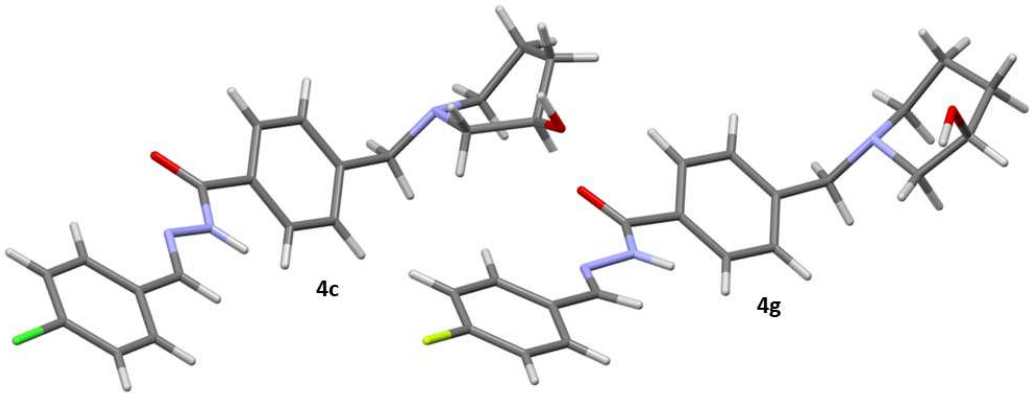

Fig. 2. Crystallographic structures of compounds **4c** (A) and **4g** (B) obtained by X-Ray power diffraction analysis.

2.2. *In Vitro* Inhibition of AChE and BuChE

All fifteen *N*-benzyl-piperidine-acylhydrazone derivatives were first screened for AChE inhibition.[44] The purified enzyme from *Electrophorus electricus* (EeAChE) was chosen for these assays because of its high similarity to human AChE (100% identity of residues lining the catalytic gorge[45] and relative low cost). Twelve compounds inhibited EeAChE by more than 60% at 100 µM (Supporting Infomation, Fig. SI1) and the 3-hydroxy-piperidine derivatives were clearly more active. Concentration-response curves for all the twenty compounds confirmed acceptable potencies and full inhibition of AChE, with the lowest IC_{50} of 2.7 µM, obtained for compound the *para*-nitrobenzyl derivative **4d** (Table 1). The different benzyl substitutions generally increased potency relative to the unsubstituted compound **4a** (IC_{50} 30.0 µM). The differences in potency among the *para*-halogenated derivatives were modest (3-fold maximum) and the potency rank was F > Br > Cl, perhaps suggesting that factors other than size were more relevant to the interaction. Seven 3-hydroxy piperidine derivatives were further evaluated for selectivity and mechanism of AChE inhibition (Supporting Information, Fig. SI2 and Fig. SI3). Assays of equine serum butyrylcholinesterase (eqBuChE) activity showed complete concentration-dependent inhibition and yielded the corresponding IC_{50} (Table 1). All tested compounds were 1.8 to 12.5 times more potent at inhibiting EeAChE than eqBuChE, with the *para*-nitrobenzyl derivative **4d** being the most selective. In the EeAChE assays of mechanism,

none of the compounds showed a significant competitive behavior towards the substrate, based on kinetic modeling of inhibition data as illustrated in Fig. 3 for compound **4g**. The simple (pure) noncompetitive inhibition model in which only V_{max} is reduced without differences in affinity for free and substrate-bound enzyme was consistently more likely than mixed inhibition models, based on the corrected Akaike information criterion (AICc). Accordingly, there were no marked differences between estimated K_i and IC_{50} (Table 1). Only for compound **4l** the probability of correctness of mixed inhibition was close to that of pure noncompetitive inhibition.

Table 1: Potency, selectivity and mechanism of action of compounds **4a-o** in cholinesterase inhibition

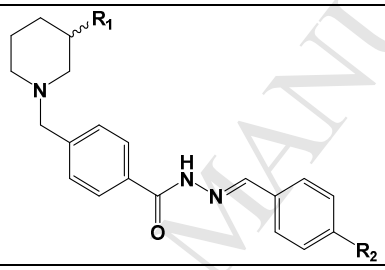

Compounds	R_1	R_2	EeAChE IC_{50} (μM)[a]	eqBuChE IC_{50} (μM)[a]	IC_{50} ratio[b]	EeAChE K_i (μM)[c]	model P ratio[dc]
4a	OH	H	30.01				
4b	OH	Br	11.89				
4c	OH	Cl	25.39	48.22	1.9	7.76	2.9
4d	OH	NO_2	2.71	33.86	12.5	2.45	3.1
4e	OH	OCH_3	13.19	91.85	7.0	11.45	3.3
4f	OH	Pyrrolidinyl	14.73				
4g	OH	F	8.65	39.04	4.5	13.41	3.3
4h	OH	NH_2	21.46				
4i	OH	Morpholinyl	≥100				
4j	OH	Piperidinyl	10.89	58.14	5.3	9.70	1.8
4k	OH	Imidazole	21.71	39.62	1.8	21.10	2.5
4l	OH	SCH_3	10.39	59.30	5.7	8.42	1.1
4m	OAc	Br	≥100				
4n	OAc	NH_2	≥100				
4o	OAc	OAc	≥100				
donepezil[e]			0.026	4.69	180		

[a]IC_{50} values are geometric means from 2-3 independent curves, each with 6 concentrations assayed in triplicates. [b]IC^{50} BuChE/IC^{50} AChE [c]Kinetic inhibition constant for the average of three independent data sets fitted to the most likely model of simple (pure) noncompetitive inhibition. [d]Ratio of probabilities of correctness of simple noncompetitive over mixed linear inhibition models, based on their AICc. Data from ref. [71].

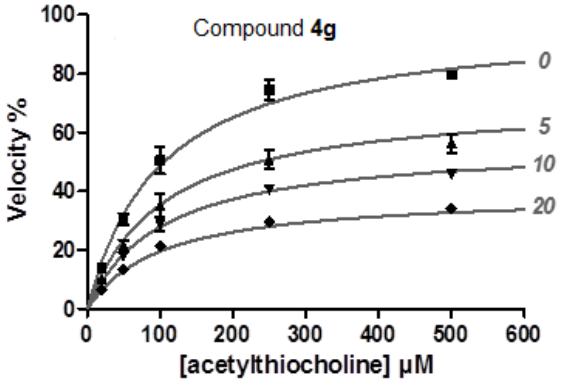

Fig. 3. Substrate competition assay of compound **4g** for EeAChE. Data points are mean ± SD from 3 independent experiments, each performed in triplicate. The curves represent the best-fitting noncompetitive inhibition model, with estimated parameters (and 95% C.I.): K_m = 101.9 (87.7 to 116.2) µM and K_i = 13.41 (11.87 to 14.96) µM. The inhibitor concentrations (µM) are indicated to the right of the curves.

2.3. Molecular docking study with human AChE

First molecular docking experiments with the inhibitor donepezil were performed into the AChE binding site to validate the three states evaluated for the enzyme (*i.e.* free, acetylated and Michaelis complex). The top ranked pose of docking experiments was compared with the experimental conformation of donepezil complexed with AChE (PDB code 4ey7). The docking simulation successfully found the experimental binding mode of donepezil in both free and acetylated forms, while for the Michaelis complex the donepezil molecule adopts a completely inverted binding mode with a significantly worse score. These results validated the structures utilized in this work, whereas the unsuccessful docking of donepezil with ACh present in the binding site might indicate that this inhibitor does not favorably interact with the Michaelis complex. Compounds **4g** and **4j**, representing halogen and heterocycle-substituted derivatives, respectively, occupy similar regions in the AChE binding site when compared with donepezil in both free and acetylated models, independent of the absolute configuration of C-3 carbon on the piperidine ring. Furthermore, the docking scores for all compounds, including donepezil, are quite similar for both free and acetylated models.

Compound **4gR** exhibited very similar binding modes for both the free and acetylated forms of AChE, mainly diverging in the position of the 3-hydroxypiperidine group and the intermolecular interaction performed by the hydroxyl group (Fig. 4A). In both situations, compound **4gR** interacts with Trp286 from the peripheral anionic site (PAS) through stacking and interacts through a hydrogen bond with Tyr124 in the middle of the enzyme gorge. In the free state, the protonated nitrogen from the 3-hydroxipiperidinyl ring interacts with Trp86 through a weak cation-π interaction and the hydroxyl group is hydrogen bonded with His447. In the acetylated enzyme, the positively charged nitrogen from the 3-hydroxipiperidinyl ring interacts with Trp86 through a stronger cation-π interaction while the hydroxyl group is hydrogen bonded to the W731.

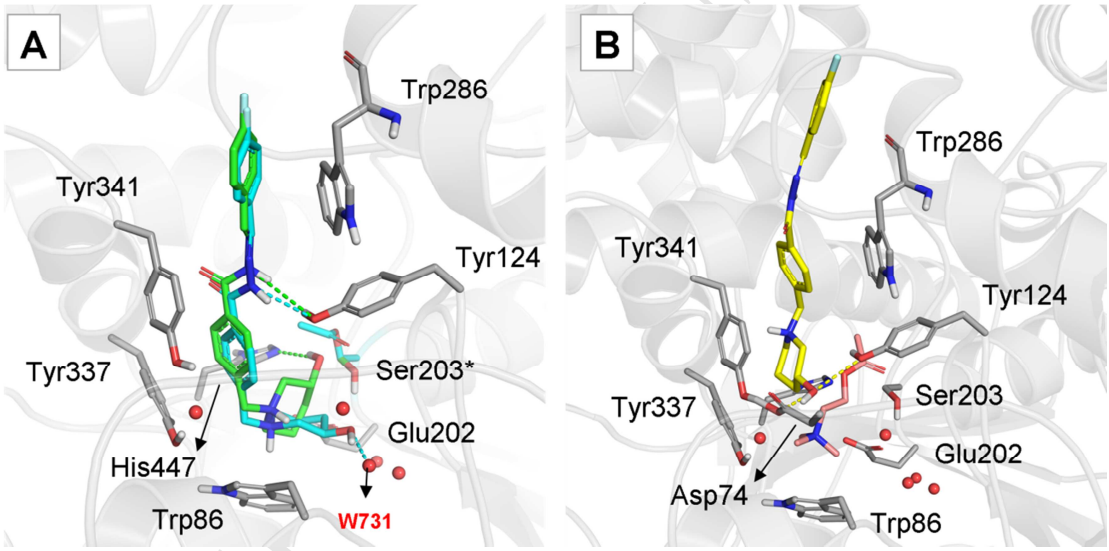

Fig. 4. Docking results for **4gR** in the (A) free (green) and acetylated (light blue) states, and in the Michaelis complex (yellow). ACh is represented as salmon sticks and molecular waters as red spheres.

The binding mode of **4g**S is almost the same for **4gR**, with a rotation of the 3-hydroxypiperidine group between the free and acetylated models (Fig. 5A). The stacking interaction between the phenyl ring and Trp286 is preserved and the hydrogen bond of the *N*-acylhydrazone (NAH) group with Trp124 is kept. The protonated nitrogen atom of the 3-hydroxypiperidine subunit is more weakly interacting through cation-π with Trp86 when compared with the R configuration and the hydroxyl group of **4gS** is hydrogen bonded to

the catalytic Ser203 or to Glu202 residues in the free and acetylated models, respectively. In the Michaelis complex (Fig. 5B) it is also possible to identify an additional binding of the 4-fluoro-phenyl subunit with ACh through van der Waals interactions and a hydrogen bond between the carbonyl group from NAH and the backbone NH of Arg296.

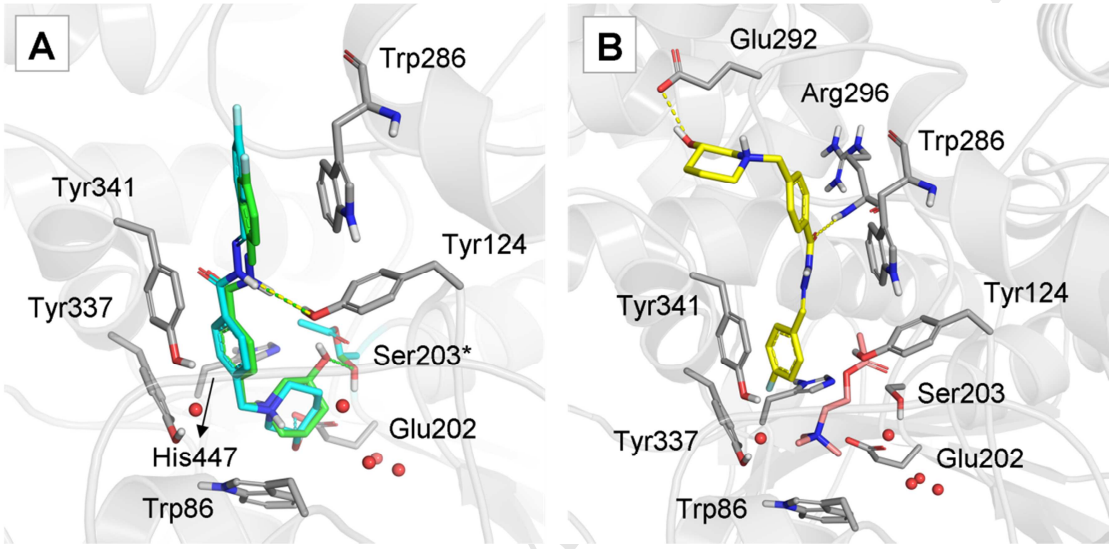

Fig. 5. Docking results for **4gS** in the (A) free (green) and acetylated (light blue) states, and in the Michaelis complex (B, yellow). ACh is represented as salmon sticks and molecular waters as red spheres.

In the Michaelis complex, the predicted binding mode for compound **4j** is significantly different for the two configurations. In the *R*-isomer (Fig. 6A), the piperidinyl group is oriented to the interior of the gorge interacting with ACh through van der Waals interactions, the protonated nitrogen is interacting with Tyr341 through cation-π and the hydroxyl group from the 3-hydroxypiperidine is interacting through a hydrogen bond with Asp74. Conversely, the *S*-isomer exhibited an inverted conformation (Fig. 5B), with the piperidine group oriented to the entrance of the gorge, the hydroxyl group hydrogen bonded with the highly exposed Glu292, and the carbonyl from NAH hydrogen bonded with the backbone NH of Arg296. The *R* configuration of compound **4j** exhibited identical binding modes in both free and acetylated forms of AChE with similar docking scores (Fig. 6A). Such interaction is composed of cation-π of the protonated nitrogen of the piperidinyl group with Trp86 (in a similar fashion with the ammonium group of ACh) and a hydrogen bond

of the hydroxyl with W731. The *N*-acylhydrazone group interacts through a hydrogen bond with Tyr124. At the entrance of the gorge, the phenyl ring makes a stacking interaction with the side chain of Trp286, a major component of the PAS.

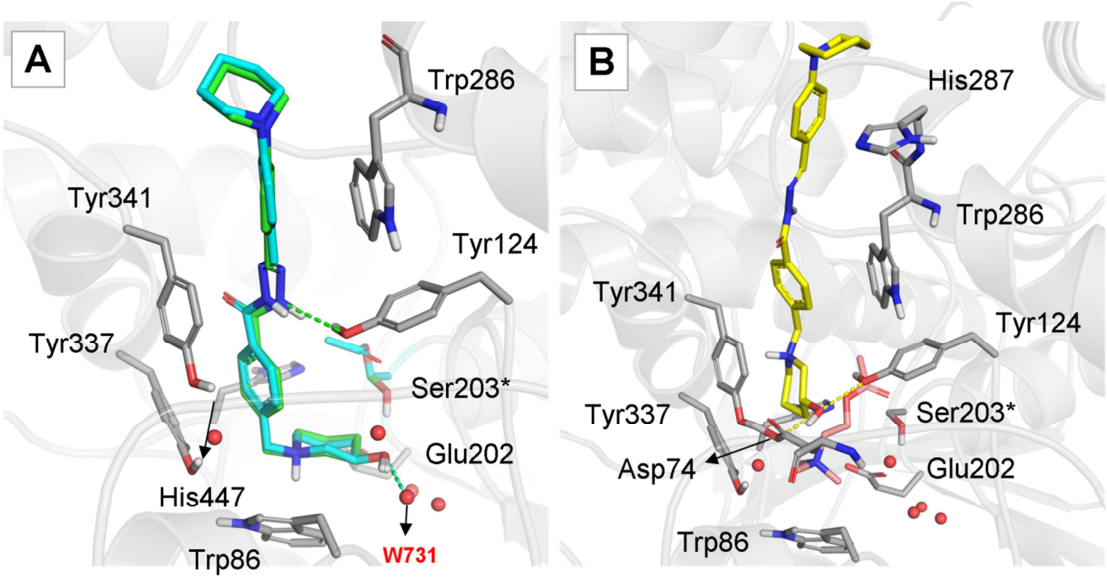

Fig. 6. Docking results for **4jR** in the (A) free (green) and acetylated (light blue) states, and in the Michaelis complex (B, yellow). ACh is represented as salmon sticks and water molecules as red spheres.

Similarly, the S enantiomer of compound **4j** exhibited almost the same binding modes in both free and acetylated states of the enzyme, with a rotation of the 3-hydroxypiperidine group at the bottom of the gorge (Fig. 7A). While the hydroxyl group is hydrogen-bonded with the catalytic Ser203 in the free enzyme, it interacts through a hydrogen bond with W737 in the acetylated model due to the steric hindrance caused by the presence of the acetyl group attached to the Ser203. In both states of the enzyme, the hydrogen atom of the charged nitrogen is pointed out to the Trp86, weakening the stacking interaction. The *N*-acylhydrazone group interacts through a hydrogen bond with Tyr124, located in the middle of the gorge, and the phenyl ring make a stacking interaction with the Trp286 indole ring at the PAS.

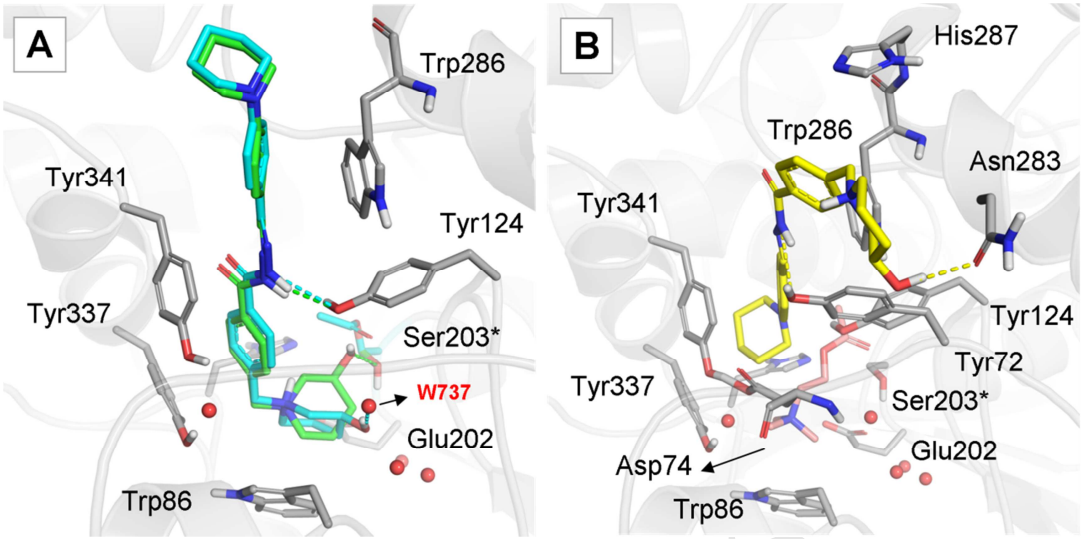

Fig. 7. Docking results for **4jS** in the (A) free (green) and acetylated (light blue) states, and in the Michaelis complex (yellow). ACh is represented as salmon sticks and water molecules as red spheres.

The predicted binding modes of both **4jR** (Fig. 6B) and **4jS** (Fig. **7**B) in the Michaelis complex are significantly distinct from those predicted in the free and acetylated models of AChE. The **4jR** binding mode exhibits the 3-hydroxypiperidine located at the bottom of the gorge, interacting with Tyr341 through cation-π interaction and with ACh through nonpolar contacts, while the hydroxyl group interacts with Tyr124 and Asp74 through hydrogen bonds. The other piperidine group is oriented to the entrance of the binding cavity, mostly exposed to the solvent. The binding mode predicted for **4jS** exhibits the 3-hydroxypiperidine group located at the entry of the gorge hydrogen bonded with the Asn283 side chain. The other piperidine group is located at the bottom of the cavity, located at hydrogen bond distance from the hydroxyl group of Tyr124 (3.13Å), and interacts with ACh through nonpolar interactions.

2.4. *In vivo* Anti-inflammatory Activity

In parallel to the AChE inhibition studies, all compounds were evaluated for their potential anti-inflammatory properties. For this purpose, classical animal models such as mechanical allodynia test, formalin-induced hyperalgesia and carrageenan-induced paw

edema assays were used as described in the literature.[46–49] Table 2 shows that eleven of the fourteen compounds evaluated (**4c**, **4e-g**, **4m**, **4n**, **4i**, **4j**, **4o** and **4l**) significantly reduced the mechanical hyperalgesic index. The seven most active compounds **4c**, **4e**, **4g**, **4i**, **4j**, **4n** and **4o** were selected for testing in the formalin test. These compounds decreased the licking time in the first (early) phase of the test, showing an analgesic effect. Compounds **4c**, **4e**, **4g**, **4i** and **4n** further reduced the licking time in the second phase of the formalin test, and they were therefore selected for the carrageenan-induced edema test All five compounds reduced edema volume, confirming an anti-inflammatory effect.

Table 2. Effect of the compounds **4b-o** in mechanical allodynia, formalin and paw edema tests.

Compound	Mechanical hyperalgesic index	Formalin		Edema	
		early phase	last phase	Volume (uL)	ID_{50} (μmol/Kg)
Saline	324.1 ± 25.2	74.00±7.7	135.8±10.7	67.73±4.2	
4b	235.8 ± 55.1				
4c	168.3 ± 46.1***	14.00±2.7***	62.88±10.7***	17.14±4.7***	8.76
4d	320.1 ± 31.3				
4e	161.1 ± 29.1***	13.29±3.2***	15.86±6.3***	25.71±2.0***	68.3
4f	206.4 ± 58.0**				
4g	178.9 ± 28.6***	18.86±3.8***	24.17±8.4***	20.00±2.1***	4.66
4h	244.4 ± 62.8				
4i	83.96 ± 26.1***	62.75±6.8***	69.67±10.7***	21.43±5.9***	2.67
4j	64.56 ± 18.8***	19.63±3.1***	110.0±21.9		
4l	260.3 ± 54.5*				
4m	206.9 ± 37.1**				
4n	146.1 ± 27.2***	47.75±13.1**	69.75±13.9**	11.43±4.0***	4.20
4o	353.1 ± 39.2				
Ind	158.1 ± 19.9***	65.43±6.8	22.75±6.5***	14.29±2.9***	2.12
Morph		7.500±1.8***	3.375±1.6***		

Each value represents the mean (±S.E.M.) of eight animals. *p < 0.05, ** p < 0.01 and *** p < 0.001 when compared with the vehicle group. Ind= indomethacin, Morph= morphine

2.5. *In vitro* and in vivo COX-1 and COX-2 Activity

Recent studies suggested that hydrazone derivatives display anti-inflammatory effects through the inhibition of cyclooxygenases 1 (COX-1) and 2 (COX-2)[50–52]. We selected compounds **4c** and **4g**, active in both AChE and anti-inflammatory assays, to evaluate their inhibition of COX-1 and COX-2 activity. As reported in Fig. 8a, compounds **4c**, **4g** and ibuprofen, used as positive control, inhibited both COX-1 (51%, 64% and 88%, respectively) and COX-2 (65%, 53% and 94%, respectively) activity at 10 µM, with a COX selectivity index (ratio of maximum inhibition on COX-2 and COX-1) of 1.27, 0.83 and 1.07, respectively. Subsequently, we also evaluated the ability of **4c** and **4g** to decrease the COX-1 and COX-2 protein levels of mice treated with the tested-compounds and carrageenan, a pro-inflammatory polysaccharide. COX-1 and COX-2 levels were measured in mice serum by using enzyme-linked immunosorbent assay. As shown in Fig.s 8b and 8c, compounds **4c** and **4g** and indomethacin, used as positive control, significantly decreased COX-1 (percentage of inhibition, 27%, 34% and 52%, respectively) and COX-2 (42%, 25% and 40%, respectively).

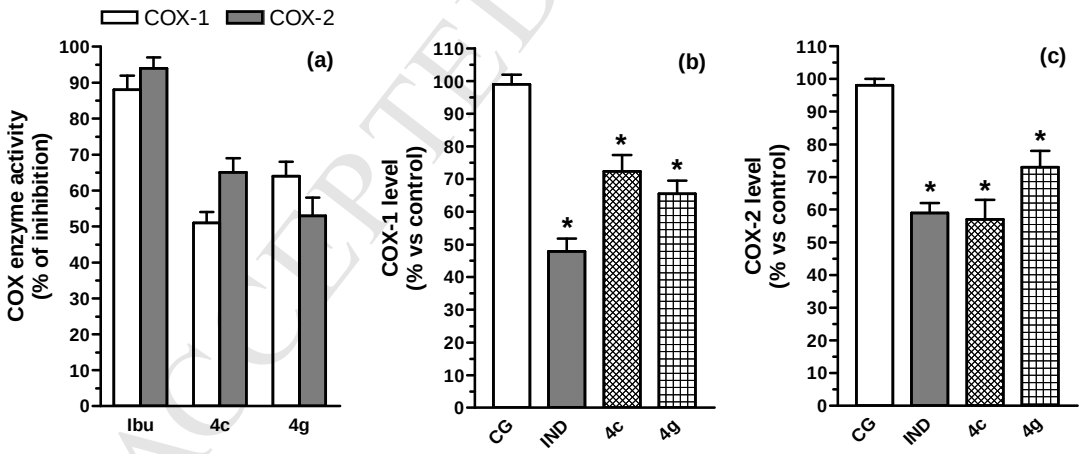

Fig. 8. Effect of compounds **4c** and **4g** on COX-1 and COX-2 enzyme activity and blood levels. (a) *In vitro* peroxidative activity of human COX-1 and ovine COX-2 was determined by a chemiluminescence assay in the presence of compounds (10 µM) or ibuprofen (Ibu), as a positive control. Values are the mean ± SEM of two independent experiments. (b, c) Plasma COX-1 and

COX-2 levels were evaluated in mice orally treated with the compounds (100 mM/kg, p.o) and then injected with carrageenan (CG) in the paw. Indomethacin (IND) was a positive control. Values are expressed as mean ± SEM (n=8) in terms of COX level percentage (*P<0.05 compared to the CG group).

2.6. Molecular docking study with COX-1 and COX-2

Considering the *in vitro* and *in vivo* anti-inflammatory results, we also studied the binding mode and selectivity *in silico* of the target compounds toward COX-1 and COX-2. According to the redocking results, the docking strategy was successfully applied to both COX-1 and COX-2, providing predicted poses similar to the experimentally observed binding mode of the reference ligands (i.e. celecoxib and rofecoxib) with RMSD values of 1.029 Å and 0.400 Å, respectively.[53–55] According to affinity predictions, the configuration *R-R* of the compounds **4c** and **4g** provide more favorable interaction with the COX-1 enzyme (it is important to note that the *R-R* configurations have very similar predicted affinities for COX-1), while *S-S* compounds interact better with COX-2 (Table 3 and **Fig.** 9).

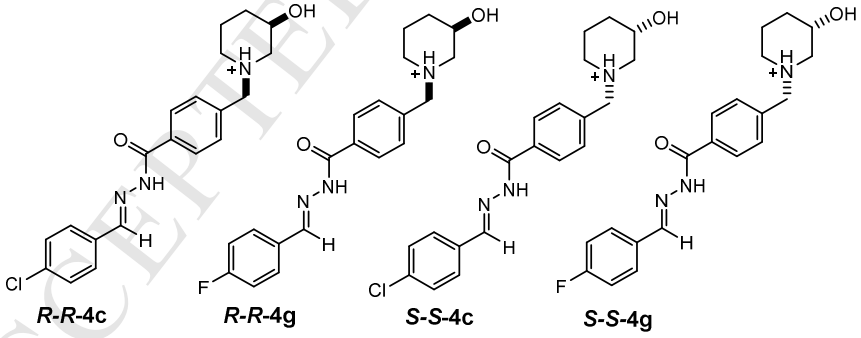

Fig. 9. 2D structures of (R-R) and (S-S) configurations of **4c** and **4g**.

Table 3. Binding affinities predicted by DockTScore for the top ranked pose of (R-R) and (S-S) compounds **4c**, **4g** and the reference ligands celeboxib and rofecoxib from docking with DockThor.

Compound	**COX-1**[a]	**COX-2**[a]
R-R- 4c	-10.427	-8.793
S-S-4c	-10.378	-10.129
R-R-4g	-10.326	-8.617
S-S-4g	-10.320	-10.080
Celeboxib	10.489	n.a.
Rofecoxib	n.a.	-10.052

[a]Given in kcal mol^{-1}.

In the computational study, both compounds **4c** and **4g** exhibited similar docking scores and binding modes in both COX-1 and COX-2 (Table 3, **Fig.** 10 and 11), interacting with the binding channel through diverse lipophilic and hydrophilic interactions. The overall binding mode is characterized by the hydroxyl-piperidine group oriented to the active site at the bottom of the channel, while halogen-phenyl ring is located at the entrance of the binding cavity exposed to the solvent. Strikingly, the piperidine amine group is located in a hydrophobic region without interacting with charged or polar atoms. We believe that this interaction is thermodynamically unfavorable and might reflect on a weakening of the affinity for both COX-1 and COX-2. Interestingly, *S*-*S*-**4c** interacts with COX-2 through four hydrogen bonds: the hydroxyl group is hydrogen-bonded with the Tyr385 side chain and the *N*-acylhydrazone is stabilized by three hydrogen bonds with Leu319, Ser320 and His90. Furthermore, the hydroxyl group of **4c** is close to the Ser530 residue, interacting through polar contacts (~ 3.8 Å). On the other hand, in COX-1, the *R*-*R* configuration lost the interaction with Tyr385 due to the rotation of the hydroxy-piperidine group.

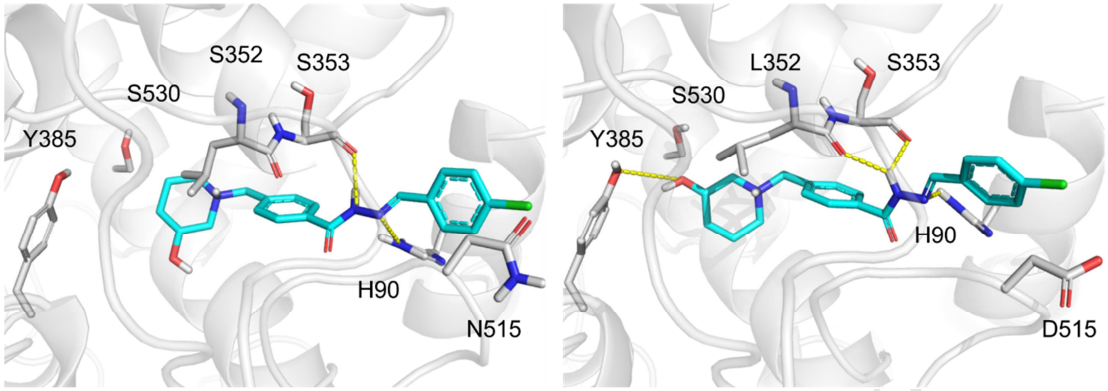

Fig. 10. Docking results of **4c** (light blue) in the COX-1 (left) and COX-2 (right) catalytic channels. Hydrogen bonds are represented as yellow dashes.

In COX-1, compound *R*-*R*-**4g** interacts through two hydrogen bonds: the *N*-acylhydrazone is hydrogen bonded with Ser353 backbone and His90 side chain. In COX-2, compound *S*-*S*-**4g** exhibits the NH from *N*-acylhydrazone interacting with Leu319 and Ser320 backbones through two hydrogen bonds, while the hydroxyl group is oriented toward the side chains of Ser530 and Tyr385 residues due to the rotation of the hydroxyl-piperidine subunit (Fig. 10).

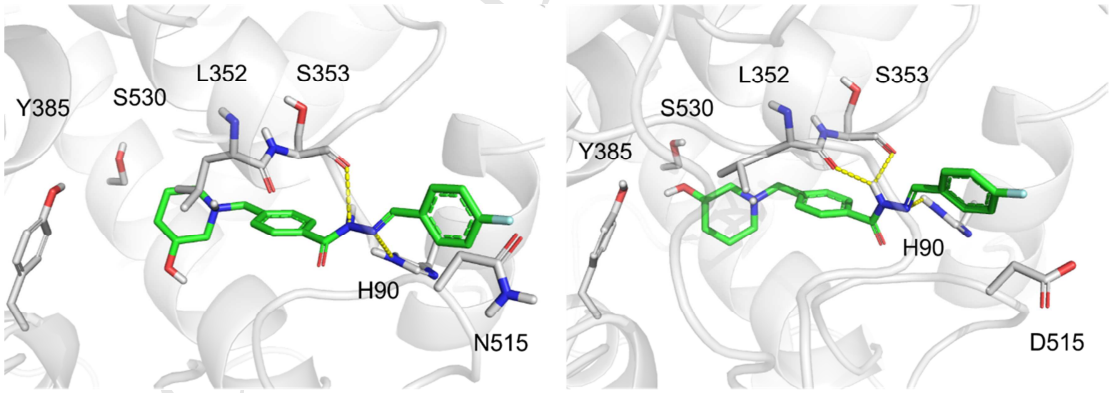

Fig. 11. Docking results of **4g** (light green) in the COX-1 (left) and COX-2 (right) catalytic channels. Hydrogen bonds are represented as yellow dashes.

2.7. Toxicity profile in vitro and ADME prediction and in silico.

Cytotoxicity and genotoxicity of the most promising compounds **4c** and **4g** was evaluated in peripheral blood mononuclear (PBMC) cells, liver HepG2 and neuronal SH-SY5Y cells. Initially, the IC_{50} (concentration of the compound resulting in 50% inhibition of cell viability) values were determined after a 6 h treatment of PBMCs and HepG2 cells, and a 24 h treatment of SH-SY5Y cells by MTT assay. As shown in Table 4, the compounds were not toxic to any type of cells up to the highest tested concentration (100 µM for PBMCs and HepG2 cells; 80 µM for SH-SY5Y cells). Subsequently, we also determined the genotoxicity to HepG2cells of low concentrations of compounds **4c** and **4g** (20 µM or 40 µM), using the comet assay and micronucleus (MN) test. The electrophoretic formation of nuclear DNA "tail" and the occurrence of micronuclei reflect DNA damage and clastogenicity/aneugenicity, respectively [56,57]. Remarkably, the treatment of HepG2 cells with **4c** and **4g** did not induce any genotoxic effects (Table 4).

Table 4. *In vitro* cytotoxicity and genotoxicity profile of compound **4c** and **4g**

Compounds	**Cytotoxicity[a] (IC_{50}, µM)[b]**			**Genotoxicity[c]**	
	PBMCs	**HepG2 cells**	**SH-SY5Y cells**	**Tail moment**	**MNi**
Control				10	26
4c	>100	> 80	> 80	10	23
4g	>100	> 80	> 80	14	24
Donepezil	n.d.[d]	n.d.	n.d.	12	24
Doxorubicin	n.d.	n.d.	n.d.	35[e]	45[f]
Ultraviolet light	n.d.	n.d.	n.d.	138[e]	n.d.

[a]Cytotoxicity was evaluated in PBMC, HepG2 and SH-SY5Y cells as reported in experimental section. [b]IC_{50} values represent the concentration of the compound resulting in 50% inhibition of cell viability; the values are the mean of two/three independent determinations. [c]Genotoxicity was determined in HepG2 cells after treatment with compounds (20 µM or 40 µM) in terms of comet tail moment (DNA damage parameter) and micronuclei index (MNi, clastogenicity/aneugenicity parameter). [d]n.d.: not determined; [e]$p<0.001$ versus untreated HepG2 cells (control); [f]$p<0.05$ versus untreated HepG2 cells (control).

In addition, some relevant ADME parameters were also predicted *in silico* by using the QikProp v. 3.5 (Schrödinger). Our data indicate that the most promising multifunctional

compounds **4c** and **4g** are in accordance with the software reference parameters (data shown in the Supporting Information, Table SI1), with adequate clogP and water solubility, and good predicted serum albumin binding, human absorption and blood-brain barrier transposition in comparison to donepezil, included as reference drug.

2.8. In vitro and in vivo neuroprotective activity

Among the different forms of Aβ aggregates, soluble Aβ oligomers (AβO) cause a selective synaptic dysfunction and/or neuronal loss in cortex and hippocampus, two stricken brain regions in AD[58,59]. AβOs display higher hydrophobicity and ability to interact with and cross the membranes, leading to formation of ion channels, membrane disruption and mitochondrial dysfunction with neuronal death[60]. In addition, AβOs exacerbate responses from glial cells with the overproduction of inflammatory cytokines, glutamatergic excitotoxicity, neuroinflammation and loss of synaptic function[61,62]. In this regard, we evaluated the effects of compound **4c** and **4g** in *in vitro* and *in vivo* models of neuroinflammation and neurodegeneration induced by either LPS or $A\beta_{1-42}$ oligomers ($A\beta_{1-42}O$). First, we evaluated the ability of compounds **4c** and **4g** to counteract the release of pro-inflammatory factors, such as TNFα and IL-1β, from human THP-1 cells activated by LPS. The THP-1 cells are transformed monocytes that have a range of properties similar to microglia, including release of superoxide anion, TNFα, IL-1β and PGE_2[63]. The treatment of THP-1 cells for 24 h with 10 μM of either compound **4c** or **4g** significantly inhibited the LPS-elicited release of both TNFα (98% and 69%, respectively) and IL-1β (29% and 31%, respectively) (Fig. 12). Anti-neuroinflammatory effects were then confirmed *in vivo*, in mice subjected to unilateral intrahippocampal injection $A\beta_{1-42}O$. The intraperitoneal administration of either compound **4c** or **4g** determined a significant reduction of Iba-1 immunostaining, a marker of activated microglia, in the CA1 area of the ipsilateral hippocampus, suggesting that both compounds reduced $A\beta_{1-42}O$ -evoked neuroinflammation (Fig. 13a/b). Iba-1 immunostaining in the CA1 area of contralateral hippocampus was not affected by any treatment, confirming the selective unilateral effect of the intrahippocampal $A\beta_{1-42}O$ injection and the lack of systemic pro-inflammatory effects of the compounds in mice (Fig. 13a/b).

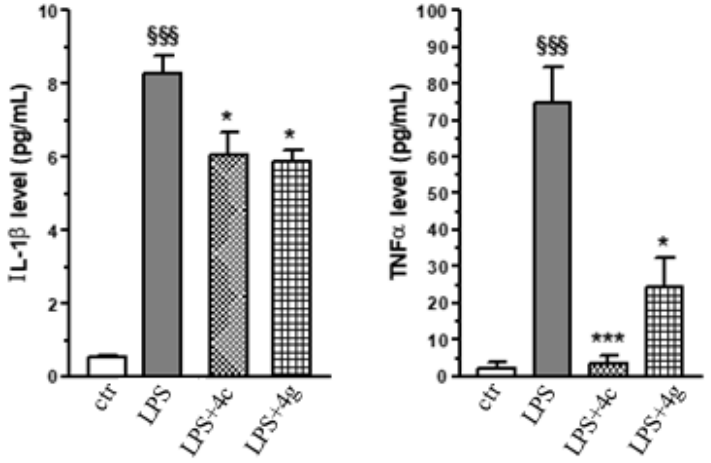

Fig. 12. Compounds **4c** and **4g** inhibit the release of TNFα and IL-1β induced by LPS in THP-1 cells, representative of human microglial cells. THP-1 cells were treated with compounds (10 μM) and LPS (1 μg/mL) for 24 h. At the end of the treatment, the pro-inflammatory cytokine levels were determined as described in the experimental section. The values are reported as mean ± SD of three independent experiments. $^{§§§}p < 0.001$ vs. untreated cells, $^{*}p < 0.05$ and $^{***}p < 0.001$ vs. cells treated with LPS (ANOVA with Bonferroni post hoc test).

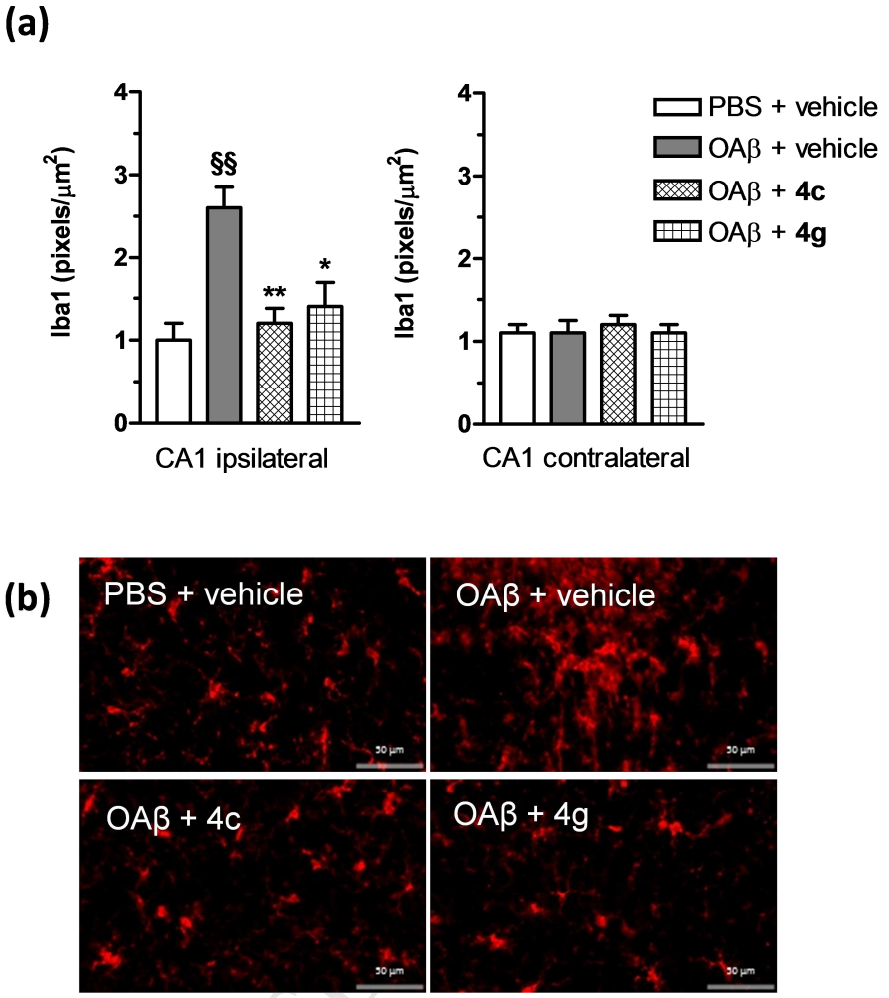

Fig. 13. Compounds **4c** and **4g** inhibit microgliosis induced by unilateral intrahippocampal injection of $A\beta_{1-42}O$ in mice. (a) The quantitative analysis of microgliosis in the CA1 area of the ipsilateral and contralateral hippocampus by Iba1 immunostaining was performed 7 days after the administration of compound (100 mg/kg, i.p.) and $A\beta_{1-42}O$ intrahippocampal injection in mice as reported in the experimental section. (b) Representative Iba1 immunostaining of the hippocampus. Scale bar 50 μm. Values are expressed as mean ± SEM (n = 10) of the pixel density of each image analyzed. $^{§§}p<0.01$ vs. PBS + vehicle; *p < 0.05 and **p < 0.01 vs. Aβ + vehicle; ANOVA, with Newman-Keuls post hoc test.

In parallel, we determined the ability of compounds **4c** and **4g** to counteract the early and late neurotoxic events, in terms of MTT formazan exocytosis and necrosis elicited by $A\beta_{1-42}O$ in neuronal SH-SY5Y cells. In particular, MTT formazan exocytosis induced by $A\beta_{1-42}O$ reveals an early vacuole formation prodromic to neuronal death[64]. Ten

micromolar of compound **4c** significantly decreased both MTT formazan exocytosis and neuronal death elicited by $A\beta_{1-42}O$ in neuronal SH-SY5Y cells. In contrast to **4c**, compound **4g** showed only the ability to significantly counteract the late neuronal death elicited by $A\beta_{1-42}$ (Fig. 14). These results reveal the best *in vitro* neuroprotective activity of **4c,** suggesting its ability to interfere with intracellular signal transduction pathways by which Aβ enhances early MTT formazan exocytosis.

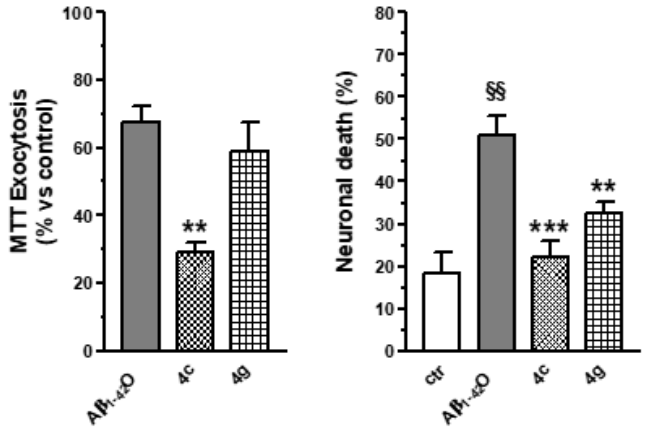

Fig. 14. Effects of compound **4c** and **4g** on early and late neurotoxic events, in terms of MTT formazan exocytosis and neuronal death elicited by $A\beta_{1-42}O$ in neuronal SH-SY5Y cells. The cells were treated with the compounds (10 μM) and $A\beta_{1-42}O$ (10 μM) for increasing amounts time. At the end of the treatment of 4 and 24 h, MTT formazan exocytosis and neuronal death were determined using MTT and propidium iodide, respectively, as described in the experimental section. The values are reported as mean ± SD of three independent experiments. $^{§§}p<0.01$ vs, untreated cells, $^{**}p<0.01$ and $^{***}p<0.001$ vs. cells treated with $A\beta_{1-42}O$, at ANOVA with Bonferroni post hoc test.

Subsequently, we evaluated the neuroprotective effects of compounds **4c** and **4g** against neurodegeneration induced by unilateral intrahippocampal injection of $A\beta_{1-42}O$ in mice. After the administration of the compounds we determined the neurodegeneration in the CA1 area of the ipsilateral hippocampus using Fluoro-Jade C (FJC), a marker of neuronal death. As shown in Fig. 15, there was a trend towards a reduction in FJC staining by the compound **4c** in CA1 area of the ipsilateral hippocampus highlighting that only compound **4c** counteracts the Aβ induced neuronal death. There was no significant change in neuronal death in the CA1 area of the contralateral hippocampus among the groups

injected with PBS, Aβ or Aβ treated with **4c**. On the other hand, the compound **4g** increased the neurodegeneration in both hippocampi, suggesting that its lack of *in vivo* neuroprotective effect could be ascribed to its in vivo intrinsic neurotoxic effects.

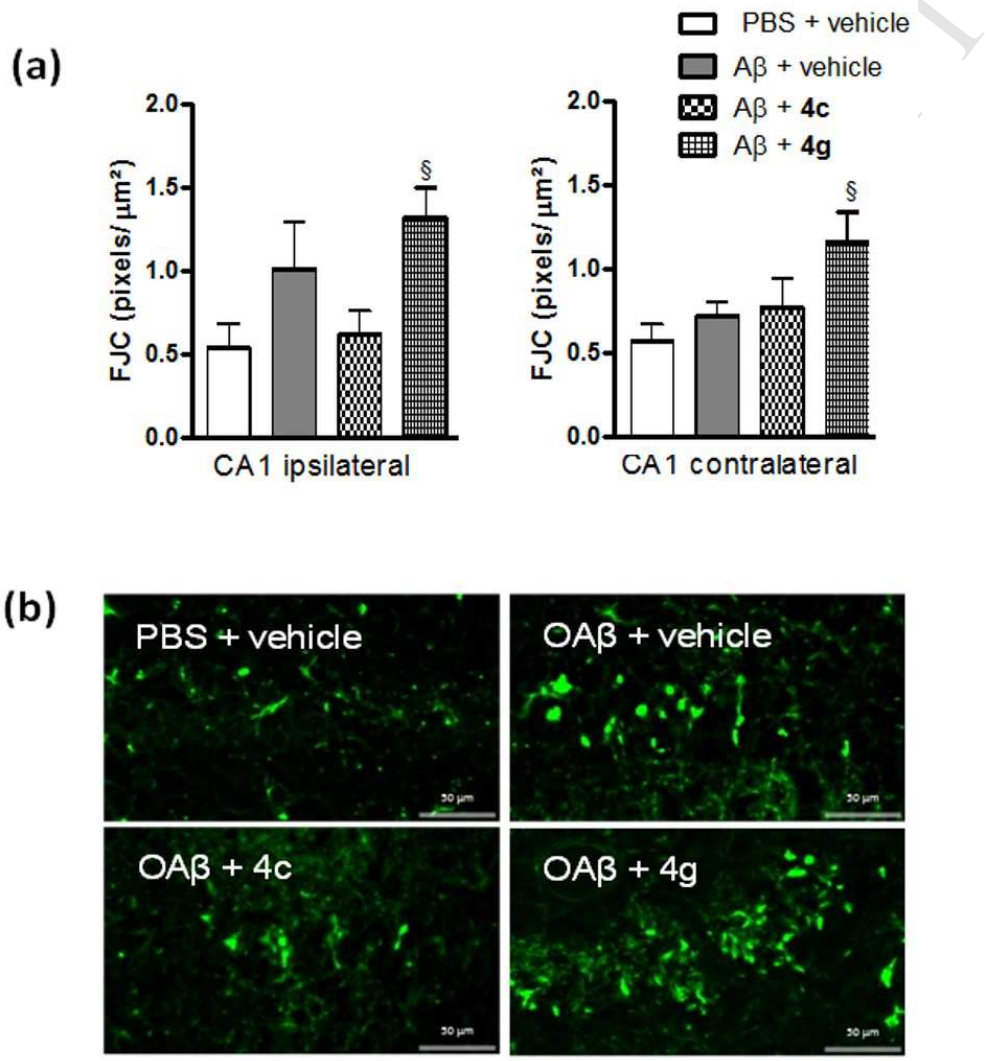

Fig. 15. Compounds **4c**, but not **4g**, counteract the neuronal death induced by unilateral intrahippocampal injection of $A\beta_{1\text{-}42}O$ in mice. (a) The quantitative analysis of neuronal death in the CA1 area of the ipsilateral and contralateral hippocampus by FJC staining was performed 7 days after the administration of the compounds (100 mg/kg, i.p.) and $A\beta_{1\text{-}42}O$ intrahippocampal injection in mice as reported in experimental section. (b) Representative FJC staining of hippocampus slices. Scale bar 50 µm. Values are expressed as mean ± SEM (n= 10) of the pixel intensity of each hippocampus slice analyzed. $^{\S}p<0.05$ vs. PBS + vehicle; *p < 0.05 vs. AβO + vehicle; ANOVA, with Newman-Keuls post hoc test.

3. Experimental section

3.1. Chemistry.

Reagents were obtained from Sigma-Aldrich, Acros or Merck. The solvents were prepared by standard procedures. Analytical thin-layer chromatography (TLC) was performed using silica 60 F254 from Merck and spots were visualized with UV light. Melting points were measured in capillary tubes on a Marte (PFM II) melting point apparatus without correction. Nuclear magnetic resonance (NMR) spectroscopy was performed on a Bruker AC-300 NMR (IS as TMS). Chemical shifts were reported in parts per million (ppm, δ) downfield from tetramethylsilane. Proton coupling patterns were described as singlet (s), doublet (d), triplet (t), quartet (q) and multiplet (m). High-resolution mass spectra (HRMS) were obtained by electrospray ionization (ESI) using a Agilent 6550 iFunnel Q-TOF LC/MS. Infrared (IR) spectra were obtained by Nicolet iS50 FTIR (Thermo Scientific USA) infrared spectrometer coupled to Pike Gladi ATR Technologies. The absorption bands were reported in wave numbers (cm^{-1}, ν). All spectra are available in supporting information (Fig. SI4 – Fig. SI72).

3.1.1. Methyl 4-formylbenzoate (6).

A solution of 4-formylbenzoic acid (**5**, 1g, 6.78mmol), catalytic DMF, $SOCl_2$ (2 mL, 27.26 mmol) in dichloromethane (10mL) was stirred and refluxed for 40 minutes, than methanol in excess was added. The solution was stirred and refluxed for additional 1 hour. Removal of the solvents produced a residue which was purified using column chromatography, eluted with a mixture of EtOAc/EtOH (8:2) to afford compound **6** as a white solid in 87% yield. ^{1}H NMR (CD_3OD, 300MHz): δ 10.06 (s, 1H), 8.16 (d, *J*=8.0Hz, 2H), 7.97 (d, *J*= 10.0Hz, 2H), 3.93 (s, 3H). ^{13}C NMR (CD_3OD, 75 MHz): δ 191.6, 166.4, 139.0, 134.6, 129.2, 128.7, 128.5, 128.4, 51.7. IR: *ν* 3300, 2500, 2835, 2735, 2997, 2954, 1724, 1707, 1280, 1111.

3.1.2. Methyl 4-((3-hydroxypiperidin-1-yl)methyl)benzoate (8).

To a mixture of methyl 4-formylbenzoate (**6**.2 g, 12.2 mmol) and piperidin-3-ol (**7**.147 g, 14.6 mmol) in methanol (10 mL) was added another mixture of zinc chloride (0.83 g, 6.1 mmol) and sodium cyanoborohydride (0.76 g, 12.2 mmol) in methanol (6 mL). The resultant mixture was stirred at room temperature for 24h. The solvent was evaporated

and water was added (40mL), followed by addition of a solution of NaOH 20% to alkalize the mixture. Then, the mixture was extracted with CH_2Cl_2 (3 × 20 mL). The organic layer was separated and dried over brine and $MgSO_4$. Removal of the solvents produced a residue which was purified using column chromatography, eluted with a mixture of EtOAc/MeOH (9:1, v/v), to afford compound **8** as a white solid. 90% yield. ^{1}H NMR (CD_3OD, 300MHz): δ 7.95 (d, *J*= 8.0Hz, 2H), 7.43 (d, *J*= 7.4Hz, 2H), 3.88 (s, 3H), 3.70-3.62 (m, 1H), 3.57 (s, 2H), 2.86-2.82 (m, 1H), 2.67-2.64 (m, 1H), 2.06-2.02 (m, 1H), 1.91-1.86 (m, 2H), 1.76-1.68 (m, 1H), 1.58-1.49 (m, 1H), 1.24-1.19 (m, 1H). ^{13}C NMR (CD_3OD, 75 MHz): δ 167.0, 143.3, 129.1, 66.5, 62.1, 60.3, 53.0, 51.20, 32.4, 22.6. IR: ν 3335, 2937, 2792, 2859, 2359, 2341, 1609, 1277, 1057.

3.1.3. 4-((3-hydroxypiperidin-1-yl)methyl)benzohydrazide (9).

To a solution of methyl 4-((3-hydroxypiperidin-1-yl)methyl)benzoate (**8**, 0.5 g, 2 mmol) in ethanol (7 mL) was added hydrazine monohydrate (11.73mL, 60mmol). The resulting mixture was refluxed and stirred for 3h. Removal of the solvents produced a residue which was purified using chromatography column, eluted with a mixture of EtOAc/MeOH (8:2, v/v) to afford the compound **9** as a white solid. 95% yield. ^{1}H NMR (CD_3OD, 300MHz): δ 7.75 (d, *J*= 7.8Hz, 2H), 7.42 (d, *J*= 7.4Hz, 2H), 3.67-3.63 (m, 1H), 3.57 (s, 2H), 2.87-2.83 (m, 1 H), 2.69-2.65 (m, 1H), 2.08-2.01 (m, 1H), 1.96-1.90 (m, 2H), 1.74-1.71 (m, 1H), 1.59-1.51 (m, 1H), 1.28-1.21 (m, 1H). ^{13}C NMR (CD_3OD, 75 MHz): δ 168.0, 141.3, 131.8, 129.2, 126.8, 66.4, 62.1, 60.2, 52.9, 32.4, 22.5. IR: ν 3296, 2939, 2815, 2360, 2341, 1611, 1548, 1303.

3.1.4. General Method for the preparation of *N*-acylhydrazones intermediates.

To solution of 4-((3-hydroxypiperidin-1-yl)methyl)benzohydrazide (**9**, 0.5 g, 2 mmol) in ethanol with catalytic amount of HCl was added the corresponding aldehyde (**10**, 2.4 mmol). The mixture was stirred for 3h at room temperature. Removal of the solvent produced a residue, which was purified using chromatography column with the appropriate eluents systems.

3.1.4.1.(*E*)-*N*'-benzylidene-4-((3-hydroxypiperidin-1-yl)methyl)benzohydrazide (4a).

Gray solid. 60% yield. Mp 152-153°C. ^{1}H NMR (CD_3OD, 300MHz): δ 8.54 (s, 1H), 8.12 (d, *J*= 8.12Hz, 2H), 7.98 (d, *J*= 7.98Hz, 2H), 7.72 (d, *J*= 7.73Hz, 2H), 7.58 (t, *J*= 7.58Hz, 3H), 3.49 (s, 2H), 3.46-3.44 (m, 1H), 3.16-3.13 (m, 1H), 3.00 (m, 1H), 2.10 (m, 1H), 2.04-2.01 (m, 2H), 1.84-1.75 (m, 1H), 1.60 (m, 1H), 1.42 (m, 1H). ^{13}C NMR (CD_3OD, 75 MHz): δ 165.1, 149.5, 132.5, 138.8, 134.1, 132.5, 165.1, 132.5, 30.2, 128.4, 65.0, 58.8, 52.9, 31.0, 21.0. IR: *v* 3331, 2939, 2817, 1644, 1522, 1283, 961, 831. HRMS (ESI) m/z calcd. $C_{20}H_{23}N_3O_2$ $[M+H]^+$: 338.1869, found 338.1868.

3.1.4.2.(*E*)-*N*'-(4-bromobenzylidene)-4-((3-hydroxypiperidin-1-yl)methyl)benzohydrazide (4b).

White solid. 52% yield. Mp 192-194ºC. ^{1}H NMR (DMSO-d_6, 300MHz): δ 11.88 (s, 1H), 8.42 (s, 1H), 7.86 (d, *J*=7.9Hz, 2H), 7.67 (s, 4H), 7.43 (d, *J*=7.4Hz 2H), 3.59-3.50 (m, $1H_7$), 3.59- 3.50 (m, 1H), 2.80- 2.75 (m, 1H), 2.65- 2.61 (m, 1H), 1.92-1.85 (m, 1H), 1.76-1.70 (m, 2H), 1.63- 1.59 (m, 1H), 1.48- 1.40 (m, 1H), 1.09- 1.03 (m, 1H). ^{13}C NMR (DMSO-d_6, 75 MHz): δ 163.5, 146.8, 143.2, 134.1, 132.3, 129.2, 128.0, 123.7, 66.0, 62.1, 61.5, 53.4, 33.6, 23.6. IR: *v* 3226, 3066, 2931, 2791, 2359, 2341, 1644, 1544, 1286, 1066, 973, 958, 815, 671. HRMS (ESI) m/z calcd. $C_{20}H_{22}BrN_3O_2$ $[M+H]^+$: 416.0974, found 416.0984.

3.1.4.3.(*E*)-*N*'-(4-chlorobenzylidene)-4-((3-hydroxypiperidin-1-yl)methyl)benzohydrazide (4c).

Pale White solid. 70% yield. Mp 177-179ºC. ^{1}H NMR (DMSO-d_6, 300MHz): δ 8.34 (s, 1H), 7.95 (d, *J*=7.9Hz, 2H), 7.83 (d, *J*=7.8Hz, 2H), 7.56 (d, *J*=7.6Hz, 2H), 7.44 (d, *J*=7.5Hz, 2H), 3.84 (m, 1H), 3.59 (s, 2H), 2.98- 2.94 (m, 1H), 2.86- 2.83 (m, 1H), 2.44-2.28 (m, 1H), 1.89- 1.86 (m, 2H), 1.65- 1.61 (m, 1H), 1.42- 1.28 (m, 2H). ^{13}C NMR (DMSO-d_6, 75 MHz): δ 163.5, 146.9, 132.4, 134.9, 133.8, 132.4, 128.1, 129.4, 66.1, 61.8, 61.0, 33.3, 23.2. IR: *v* 3196, 2940, 2361, 2341, 1651, 1279, 1087. HRMS (ESI) m/z calcd. $C_{20}H_{22}ClN_3O_2$ $[M+H]^+$: 372.1479, found 372.1409.

3.1.4.4.(*E*)-4-((3-hydroxypiperidin-1-yl)methyl)-*N*'-(4-nitrobenzylidene)benzohydrazide (4d).

Yellow solid. 71% yield. Mp 222-225ºC. ^{1}H NMR (DMSO-d_6, 300MHz): δ 8.71 (s, 1H), 8.29 (d, *J*=8.3Hz, 2H), 7.96 (d, *J*=8.0Hz, 4H), 7.44 (d, *J*=7.4Hz, 2H), 2.80- 2.77 (m, 1H), 2.76- 2.62 (m, 1H), 1.94- 1.87 (m, 1H), 1.80- 1.75 (m, 2H), 1.64- 1.59 (m, 1H), 1.48-

1.38 (m, 1H), 1.11- 1.01 (m, 1H). ^{13}C NMR (DMSO-d_6, 75 MHz): δ 163.7, 148.2, 145.5, 143.1, 141.2, 132.0, 129.2, 128.4, 124.5, 66.4, 61.3, 53.4, 33.5, 23.5. IR: *v* 3323, 2943, 2849, 1667, 1545, 1284. HRMS (ESI) m/z calcd. $C_{20}H_{22}N_4O_4$ $[M+H]^+$: 383.1719, found 383.1723.

3.1.4.5.(*E*)-4-((3-hydroxypiperidin-1-yl)methyl)-*N*'-(4-ethoxybenzylidene)benzohydrazide (4e).

Gray solid. 85% yield. Mp 217-218ºC. ^{1}H NMR (CD_3OD, 300MHz): δ 8.30 (s, 1H), 7.91 (d, *J*=7.9Hz, 2H), 7.78 (d, *J*=7.8Hz, 2H), 7.51 (d, *J*=7.5Hz, 2H), 6.99 (d, *J*=7.0Hz, 2H), 3.84 (s, 3H), 3.70 (m, 3H), 2.93- 2.88 (m, 1H), 2.77- 2.73 (m, 1H), 2.23- 2.17 (m, 1H), 2.10- 2.03 (m, 1H), 1.92- 1.56 (m, 2H), 1.92-1.77 (m, 1H), 1.35-1.28 (m, 1H). ^{13}C NMR (CD_3OD, 75 MHz): δ 162.0, 149.7, 134.4, 132.7, 131.3, 129.2, 128.1, 126.5, 113.9, 59.5, 56.4, 51.9, 54.5, 27.7, 17.5. IR: *v* 3346, 3070, 3035, 2934, 2835, 1644, 1602, 1557, 1506, 1249, 1025. HRMS (ESI) m/z calcd. $C_{21}H_{25}N_3O_3$ $[M+H]^+$: 368.1974, found 368.1892.

3.1.4.6.(*E*)-4-((3-hydroxypiperidin-1-yl)methyl)-*N*'-(4-(pyrrolidin-1-yl)benzylidene)benzohydrazide (4f).

Yellow solid. 60% yield. Mp 172-174ºC. ^{1}H NMR (C_5D_5N, 300MHz): δ 12.20 (s, 1H), 8.73 (s, 1H), 8.27 (d, *J*=8.3Hz, 2H), 7.91(d, *J*=7.9Hz, 2H), 7.48 (d, *J*=7.5Hz, 2H), 6.56 (d, *J*=6.6Hz, 2H), 4.07- 3.99 (m, 1H), 3.52-3.50 (m, 2H), 3.16- 3.12 (m, 1H), 3.07- 3.02 (m, 4H), 2.64- 2.61(m, 1H), 2.22- 1.96 (m, 4H), 1.70- 1.65 (m, 4H), 1.54- 1.48 (m, 2H). ^{13}C NMR (DMSO-d_6, 75 MHz): δ 162.9, 149.1, 142.7, 132.9, 129.1, 127.8, 121.4, 112.0, 66.5, 62.2, 61.5, 53.4, 47.7, 33.7, 25.4, 23.7. IR: *v* 3252, 3070, 3035, 2916, 2842, 2360, 2340, 1645, 1602, 1523, 1275. HRMS (ESI) m/z calcd. $C_{24}H_{30}N_4O_2$ $[M+H]^+$: 407.2447, found 407.2454.

3.1.4.7.(*E*)-*N*'-(4-fluorobenzylidene)-4-((3-hydroxypiperidin-1-yl)methyl)benzohydrazide (4g).

White solid. 59% yield. Mp 192-195ºC. ^{1}H NMR (CD_3OD, 300MHz): δ 8.39 (s, 1H), 8.00 (d, *J*=8.0Hz, 2H), 7.88 (d, *J*=7.9Hz, 2H), 7.63 (d, *J*=7.6Hz, 2H), 7.17 (d, *J*=7.2Hz, 2H), 4.08 (s, 1H), 3.90 (s, 1H), 3.09- 3.00 (m, 2H), 2.82- 2.61 (m, 2H), 2.00 (m, 1H), 1.89- 1.82 (m, 1H), 1.75- 1.72 (m, 1H), 1.54- 1.51 (m, 1H). ^{13}C NMR (DMSO-d_6, 75 MHz): δ 164.8, 163.1, 161.5, 146.5, 142.7, 131.0, 129.3, 128.7, 127.6, 116.1, 66.1, 61.7,

61.1, 53.0, 33.2, 23.2. IR: *v* 3176, 3070, 3035, 3041, 2358, 2332, 1639, 1600, 1556, 1507, 1293, 1148. HRMS (ESI) m/z calcd. $C_{20}H_{22}FN_3O_2$ $[M+H]^+$: 356.1774, found 356.1786.

3.1.4.8.(*E*)-N'-(4-aminobenzylidene)-4-((3-hydroxypiperidin-1-yl)methyl)benzohydrazide (4h).

White solid. 15% yield. Mp 125ºC. ^{1}H NMR (CD_3OD, 200MHz): δ 8.17 (s, 1H), 7.86 (d, *J*=8.0Hz, 2H), 7.48 (m, 4H), 6.67 (d, *J*=8.0Hz, 2H), 3.62 (s, 2H), 3.25 (s, 1H), 2.88-2.67 (m, 2H), 2,13-1,26 (m, 6H). ^{13}C NMR (CD_3OD, 75MHz): δ 164.9, 151.0, 141.4, 140.0, 132.0, 129.4, 129.1, 122.4, 114.0, 66.1, 61.9, 60.4, 52.9, 32.1, 22.3. IR: *v* 3348, 3228, 2852, 2922, 1651, 1597, 1056. HRMS (ESI) m/z calcd. $[M+H]^+$: 353.1978, found 353.1971.

3.1.4.9.(*E*)-4-((3-hydroxypiperidin-1-yl)methyl)-*N*'-(4-morpholinobenzylidene) benzohydrazide (4i).

Yellow solid. 54% yield. Mp 154-157ºC. ^{1}H NMR (C_5D_5N, 300MHz): δ 12.42 (s, 1H), 8.74 (s, 1H), 8.26 (d, *J*=8.3Hz, 2H), 7.94 (d, *J*=7.9, 2H), 7.51 (d, *J*=7.5Hz, 2H), 6.99 (d, *J*=7.0, 2H), 5.70 (s, 2H), 4.08- 4.02 (m, 1H), 3.74 (t, 4H), 3.55 (m, 1H), 3.12 (t, 4H), 2.66- 2.63 (m, 1H), 2.25- 2.16 (m, 1H), 2.12- 2.01 (m, 2H), 1.74- 1.48 (m, 3H). ^{13}C NMR (DMSO-d_6, 75 MHz): δ 163.1, 152.6, 148.4, 142.4, 132.8, 129.2, 128.7, 127.9, 125.0, 114.8, 66.4, 62.0, 53.4, 47.9, 33.5, 23.5. IR: *v* 3429, 3257, 2831, 2359, 2341, 1609, 1537, 1228. HRMS (ESI) m/z calcd. $C_{24}H_{30}N_4O_3$ $[M+H]^+$: 423.2396, found 423.2407.

3.1.4.10. (*E*)-4-((3-hydroxypiperidin-1-yl)methyl)-*N*'-(4-(piperidin-1-yl)benzylidene) benzohydrazide (4j).

Yellow solid. 50% yield. Mp 158-162ºC. ^{1}H NMR (C_5D_5N, 300MHz): δ 12.38 (s, 1H), 8.74 (s, 1H), 8.26 (d, *J*=8.3Hz, 2H), 7.92 (d, *J*=7.9Hz, 2H), 7.50 (d, *J*=7.5Hz, 2H), 6.97 (d, *J*=7.0Hz, 2H), 4.10-4.03 (m, 1H), 3.55 (s, 2H), 3.11 (t, *J*=3.1Hz, 4H), 2.67- 2.63 (m, 1H), 2.25- 1.98 (m, 4H), 1.74- 1.55 (m, 3H), 1. 49- 1.41 (m, 6H). ^{13}C NMR (DMSO-d_6, 75 MHz): δ 163.1, 152.8, 148.6, 142.3, 132.9, 129.2, 128.8, 127.9, 123.8, 115.0, 66.3, 61.2, 51.3, 48.8, 33.5, 25.4, 24.3, 23.4. IR: *v* 3176, 3032, 2932, 849, 1638, 1594, 1557, 1516, 1294. HRMS (ESI) m/z calcd. $C_{25}H_{32}N_4O_2$ $[M+H]^+$: 421.2604, found 421.2616.

3.1.4.11. (*E*)-*N*'-(4-(1H-imidazol-1-yl)benzylidene)-4-((3-hydroxypiperidin-1-yl)methyl)benzohydrazide (4k).

Pale white solid. 49% yield. Mp 113-114ºC. ^{1}H NMR (CD_3OD, 300MHz): δ 8.40 (s, 1H), 8.23 (s, 1H), 8.01 (d, *J*=8.0Hz, 2H), 7.93 (d, *J*=7.9Hz, 2H), 7.66 (d, *J*=7.7Hz, 3H), 7.52 (d, *J*=7.5Hz, 2H), 7.18 (s, 1H), , 3.68 (s, 3H), 2.92- 2.88 (m, 1H), 2.75- 2.72 (m, 1H), 2.19- 2.12 (m, 1H), 2.06- 2.00 (m, 1H), 1.95- 1.88 (m, 1H), 1.82- 1.76 (m, 1H), 1.64- 1.52 (m, 1H), 1.34- 1.26 (m, 1H). ^{13}C NMR (DMSO-d_6, 75 MHz): δ 163.6, 147.0, 142.8, 138.2, 133.2, 132.3, 130.5, 129.2, 128.0, 120.8, 118.3, 66.5, 62.1, 61.5, 53.4, 33.6, 23.6. IR: *v* 3430, 3252, 2925, 2832, 1644, 1608, 1598, 1515, 1229. HRMS (ESI) m/z calcd. $C_{23}H_{25}N_5O_2$ $[M+H]^+$: 404.2087, found 404.2088.

3.1.4.12. (*E*)-4-((3-hydroxypiperidin-1-yl)methyl)-*N*'-(4-(methylthio)benzylidene) benzohydrazide (4l).

Gray solid. 78% yield. Mp 215-218ºC. ^{1}H NMR (C_5D_5N, 300MHz): δ 12.58 (s, 1H), 8.74 (s, 1H), 8.26 (d, *J*=8.3Hz, 2H), 7.87 (d, *J*=7.9Hz, 2H), 7.50 (d, *J*=7.5Hz, 2H), 7.32 (d, *J*=7.3Hz, 2H), 4.04 (m, 1H), 3.52 (s, 2H), 3.16- 3.12 (m, 1H), 2.38 (s, 1H), , 2.23- 2.16 (m, 1H), 2.11- 2.07 (m, 1H), 2.02- 1.96 (m, 1H), 1.73- 1.47 (m, 3H). ^{13}C NMR (DMSO-d_6, 75 MHz): δ 163.4, 147.7, 143.1, 141.3, 132.4, 131.1, 129.1, 128.0, 127.9, 126.1, 66.5, 61.5, 53.4, 33.6, 23.7, 14.7. IR: *v* 3381, 3238, 2919, 2781, 2359, 2323, 1641, 1591, 1534, 1277. HRMS (ESI) m/z calcd. $C_{21}H_{25}N_3O_2S$ $[M+H]^+$: 384.1746, found 384.1755.

3.1.5. General Method for the preparation of acetate-derivatives.

A solution of the corresponding *N*-acylhydrazone (2 mmol), 4-dimethylaminopyridine (4-DMAP, 1 mmol) and acetic anhydride (20mmol) in chloroform (5 mL) was prepared. The solution was stirred and refluxed until the starting material was fully consumed (TLC). The solvent was removed under low pressure and the product was purified using chromatography column with appropriate eluent system.

3.1.5.1.(*E*)-1-(4-(2-(4-bromobenzylidene)hydrazine-1-carbonyl)benzyl)piperidin-3-yl acetate (4m).

Yellow solid. 60% yield. Mp 140ºC. ^{1}H NMR (CD_3OD, 300 MHz): δ 7.80 (d, *J*=8.30Hz, 2H), 7.50 (d, *J*=8.47Hz 2H), 7.40 (d, *J*=8.29Hz, 2H), 7.34 (d, *J*=8.50Hz, 2H), 7.02 (s, 1H), 4.76 (m, 1H), 3.25 (s, 2H), 2.74 (dd, *J*=10.66Hz, 1H), 2.53 (m, 1H), 2.30 (s, 3H), 2.15 (m, 2H), 1.83 (m, 1H), 1.73 (m, 1H), 1.54 (m, 1H), 1.38 (m, 1H). ^{13}C NMR (CD_3OD, 75 MHz): δ 171.9, 169.5, 157.2, 143.5, 136.9, 133.0, 130.6, 129.6, 128.0, 124.3,

92.9, 70.8, 63.2, 57.8, 54.1, 30.3, 23.6. IR: *v* 3232, 3053, 3217, 2943, 2798, 1734, 1649, 1204, 1244. HRMS (ESI) m/z calcd. $C_{22}H_{24}BrN_3O_3$ $[M+H]^+$: 458.1079, found 458.1073.

3.1.5.2.(*E*)-1-(4-(2-(4-aminobenzylidene)hydrazine-1-carbonyl)benzyl)piperidin-3-yl acetate (4n).

Yellow solid. 42% yield. Mp 220ºC. ^{1}H NMR (CD_3OD, 200MHz): δ 8,2 (s, 1H), 7.9 (d, *J*=5.0HzHz, 2H), 7.6 (d, *J*=5.0, 2H), 7.51 (d, *J*=10.0Hz, 2H), 6.72 (d, *J*=5.0 Hz, 2H), 4.83 (m, 1H), 3.67 (s, 2H), 2.84 – 2.67 (m, 2H), 2.30 (m, 2H), 2.04 (s, 3H), 1.91-1.82 (m, 2H), 1.49-1.31 (m, 2H). ^{13}C NMR (CD_3OD, 50MHz): δ 170.9, 165.8, 150.5, 141.5, 129.2, 127.3, 123, 114.1, 113.4, 69.4, 62, 56.4, 52.9, 29, 22.1, 19.7. IR: *v* 3446, 3350, 3217, 3032, 2943, 2802, 1722, 1649, 1264, 1248. HRMS (ESI) m/z calcd. $C_{22}H_{26}N_4O_3$ $[M+H]^+$: 395.2083, found 395.2077.

3.1.5.3.(*E*)-1-(4-(2-(4-acetoxybenzylidene)hydrazine-1-carbonyl)benzyl)piperidin-3-yl acetate (4o).

Yellow solid. 37% yield. Mp 145ºC. ^{1}H NMR (CD_3OD, 300 MHz): δ 7.83 (d, J=8.31Hz, 2H), 7.49 (d, J=8.61Hz, 2H), 7.43 (d, J=8.28Hz, 2H), 7.15 (d, J=8.62Hz, 2H), 7.09 (s, 1H), 4.78 (m, 1H), 3.58 (s, 2H), 2.77 (dd, J=10.87Hz, 1H), 2.58 (m, 1H), 2.32 (s, 3H), 2.25 (s, 3H), 2.17 (m, 1H), 1.80 (m, 2H), 1.57 (m, 1H), 1.42 (m, 1H), 1.23 (m, 1H). ^{13}C NMR (CD_3OD, 75 MHz): δ 170.8, 169.6, 157.4, 153.4, 143.3, 135.3, 130,8, 129.0, 128.0, 124.5, 123.3, 116.5, 93.2, 70.8, 63.3, 57.8, 54.2, 30.2, 23.6, 21.1. IR: *v* 3248, 3070, 2947, 2798, 1762, 1732, 1656, 1282, 1251, 1222. HRMS (ESI) m/z calcd. $C_{24}H_{27}N_3O_5$ $[M+H]^+$: 438.2029, found 438.2023.

3.2. X-Ray Diffraction.

The compounds **4c** and **4g** samples were loaded between two acetate-cellulose foils (thickness of 0.014 mm and density of 1.3 gcm-3) and the X-ray powder diffraction data were recorded at room temperature on a STADI-P powder diffractometer, (Stoe®, Darmstadt, Germany) in transmission geometry by using $CuK\alpha_1$ radiation (λ= 1.54056 Å), selected by a curved monochromator Ge (111), with a tube voltage of 40 kV and a current of 40 mA. The measurements were performed in the angular range from 4° to 82.735° (2θ) with steps of 0.015° and integration time of 200 s at each 1.05°.

3.3. Pharmacology. Cholinesterase inhibition.

Enzyme activity of EeAChE (E.C. 3.1.1.7, type V-S, purified from *Electrophorus electricus*) and eqBuChE (E.C. 3.1.1.8, purified from equine serum) was assayed kinetically by Ellman's method[44] in 96-well plates, as previously described[65,66], with minor modifications. Compound samples were dissolved at 0.05 M in DMSO and diluted in sodium phosphate buffer (SPB, 0.1 M, pH 7.4) immediately before use (final DMSO less than 0.2% v.v.). All other assay reagents were dissolved in SPB. The final assay volume was 200 µL; three wells were used per condition in each experiment. Sequential additions were: 20 µL of enzyme (0.5 U/mL), 5 µL of 5,5'-dithiobis-(2-nitrobenzoic) acid (10 mM), 100 µL of compound solution (twice the final concentration) and 55 µL of SPB. After ten minutes of incubation, 20 µL of the substrate (acetylthiocholine or butyrylthiocholine iodide, 0.5 M final) were added and absorbance was read in a SpectraMax 250 spectrophotometer (Molecular Devices) at 412 nm every 12 s, for 5 min at rt. Progression curves were acquired through SOFTmax PRO 5.0 (Molecular Devices) from which maximum hydrolysis velocity was estimated and analysis performed with Prism (Graphpad). Three six-point inhibition curves were obtained independently for each compound for estimation of average IC_{50}. The substrate competition data from three experiments were pooled and analyzed by global nonlinear fitting of standard kinetic models[66]. Because all compounds clearly reduced EeAChE V_{max}, only simple (pure) noncompetitive and linear mixed inhibition models were fitted, being then compared and selected by likelihood criteria (corrected Akaike information criterion). All reagents were purchased from Sigma-Aldrich (Brazil).

3.4. Evaluation of cytotoxicity in vitro.

The cytotoxicity of the test compounds was determined in human peripheral blood mononuclear cells (PBMCs), human liver HepG2 and neuronal SH-SY5Y cells using the 3-(4,5-dimethylthiazol-2-yl)-2,5-diphenyl tetrazolium bromide (MTT) assay. MTT is reduced to formazan by the mitochondrial activity of viable cells. PBMCs were obtained from blood of healthy volunteers by Ficoll–Hypaque density gradient centrifugation. The cell suspension of PBMCs at a concentration of 2.0×10^6 cells/mL was distributed in a 96-well plate, 90 µL in each well with 10 µL of test compounds at different final concentrations (1-100 µM), incubated at 37 °C in 5% CO_2 for 48 h. At the end of the treatment, 10 µL of

MTT (5 mg/mL) was added and the cells were incubated again for an additional 4 h period. Then, the medium was carefully removed and 100 µL of DMSO was added for solubilization of formazan crystals. The amount of formazan was measured at 570 nm (reference filter 690 nm) using a VICTOR™ X3 multilabel plate reader (PerkinElmer, MA, USA). HepG2 and SH-SY5Y cells were seeded at 1×10^4 and 2×10^4 cells/well, respectively, into a 96-well plate. After 24 h of incubation, HepG2 and SH-SY5Y cells were treated with different concentrations of test compounds (1 - 80 µM) for 6 and 24 h, respectively. At the end of the treatment, the medium was replaced with MTT (5 mg/ml) in phosphate-buffered saline (PBS) for 2 h at 37°C in 5% CO_2. After washing with PBS, the formazan crystals were dissolved with isopropanol. The amount of formazan was measured as reported above for PBMCs. In all determinations, cytotoxicity is expressed as concentration of the compound resulting in 50% inhibition of cell viability.

3.5. Evaluation of genotoxicity in vitro. Alkaline comet assay.

This assay was performed as described previously by Singh et al.[56] with some modifications. Briefly, HepG2 cells were seeded in tissue culture flasks and incubated for 6 h with test compounds at 20 µM or 40 µM. After drug treatment, the cell cultures were washed with PBS and collected by enzymatic digestion (0.05% trypsin/0.02% EDTA in PBS), and cell viability was determined by trypan blue exclusion assay. All treated cultures showed greater than 90% of viability. Cell suspensions were kept on ice and protected from the light. Two hundred thousand viable cells were resuspended in 100 µL of 0.5 % low-melting point agarose (Sigma-Aldrich) at 37˚C and mixture was spread onto microscope slides pre-coated with 1.5% normal-melting point agarose (Sigma-Aldrich). Triplicates slides were prepared for each sample. Coverslips were placed on the gel and then kept for 10 min in a refrigerator for agarose solidification. Next, the coverslips were gently removed and the slides were immersed in cold (4 °C) lysis solution (1 % Triton X-100, 10 % DMSO, 2.5 mM NaCl, 100 mM Na_2EDTA, 100 mM Tris, pH 10) for 24 h. Immediately after this step, slides were placed in a horizontal electrophoresis unit containing freshly prepared electrophoresis buffer (1 mM Na_2EDTA, 300 mM NaOH, pH 13). DNA was allowed to unwind for 20 min, and subsequently, electrophoresis was performed at 25 V, 300 mA for 25 min. The slides were then gently immersed in a neutralization buffer (0.4 M Tris–HCl,

pH 7.5) for 15 min and fixed with ethanol. Samples were stained with SYBR® Green I solution (Invitrogen by Thermo Fisher Scientific Inc., Rockford, IL, USA) diluted 1:100 in 1 × PBS and analyzed by fluorescence microscope using a 20 × objective. The images were captured and analyzed using the ImageJ open comet program (ImageJ, Wayne Rasband, National Institutes of Health, USA) to demarcate the "head" and the "tail" regions of each comet[67]. Fifty randomly selected nuclei were analyzed per slide. The extent of DNA damage (tail moment) was expressed as the mean ± SD from 3 independent experiments. Doxorubicin and ultraviolet light were used as positive control.

3.6. Cytokinesis block micronucleus assay (CBMN).

The micronucleus assay was performed according to Natarajan and Darroudi [68] with some minor modifications. Briefly, cells were seeded at a density of 2.5×10^5 cells per well in 6-well culture plates and treated for 6 h with test compounds at 20 µM or 40 µM. After the exposure period, cells were washed twice with PBS and re-incubated in fresh medium containing 3 µg/mL of cytochalasin B (Sigma-Aldrich) for 28 h. After that, cells were harvested and suspended in cold sodium citrate (1%) at room temperature for 5 min. Then, the cells were fixed in Carnoy's solution (1:3 mixtures of acetic acid and methanol), and a few drops of formaldehyde were added to preserve the cytoplasm. Immediately after centrifugation at 1000 rpm for 5 min, the cells were re-suspended in Carnoy's solution and dropped onto clean microscopic slides, air dried, and stained with Giemsa (5%). Analysis of micronuclei (MNi) was performed using a light microscope at 1,000 x magnification (immersion oil) according to the criteria published by Fenech[69,70]. Doxorubucin was used as a positive control.

3.7. Evaluation of anti-inflammatory activity in vivo.

Adult male Swiss mice (22-28 g) were obtained from the Central Animal Facility of the Federal University of Alfenas and housed under controlled light (12:12 h light-dark cycle; lights on at 6:00 a.m.) and temperature conditions (23 ± 1 °C) with access to water and food ad libitum. Except for the night before the experiments, when they were submitted to overnight fast. The animals were allowed to habituate to the housing facilities for at least

1 week before the experiments began. The experimental protocol was approved by the local Research Ethics Committee of the Federal University of Alfenas (protocol n 633/2015).

3.8. Formalin-induced nociception.

A formalin solution (5% in 0.9% saline) was injected (20 µl/paw) into the sub-plantar region of the right hind paw, and the animals were individually placed in transparent observation chambers, as previously described[71]. Oral treatments (p.o) with vehicle, indomethacin and compounds (100 mM/kg) were given 1 h prior to formalin injection (n=8 per group). Morphine (39 mM/kg) was administrated (i.p.) 30 min before the test. Animals were observed from 0 to 5 min (neurogenic pain) and from 20 to 30 min (inflammatory pain) after the formalin injection, and the time spent licking the injected paw was recorded and considered as indicative of nociception.

3.9. Mechanical nociception test.

The mechanical nociceptive thresholds of the animals was evaluated according to the up-and-down method using Von Frey filaments (North Coast Medical, Inc. Morgan Hill, CA, USA) as previously described[71]. The mice were placed in acrylic boxes with a wire screen, providing access to the paw of the animals 60 min before test. The Von Frey filaments were applied perpendicularly on the plantar region outside of the hind paw of animals, for a period of approximately 4s or until the animal demonstrates nocifensive behavior, characterized by paw withdrawal, then licking and/or “flinching”. The evaluation of mice began with the 0.4 g filament. In this method, at least 6 tests, with 10s intervals, were made per animal. The absence of animal's response to a particular filament led to the use of other filament of greater mass, until there is a withdrawal response. Vehicle, compounds or indomethacin was orally administered 1 h before the intraplantar injection of carrageenan (100 mg/paw). The results are expressed by the average nociceptive threshold in grams.

3.10. Carrageenan-induced paw edema.

Mice paw edema was measured with a plethysmometer (Ugo Basile, mod 7140) as previously described[71]. The basal volume of the right hind paw was determined before

the administration of any drug and the animals were divided into experimental groups (n=10 per groups) in such a way that the mean volumes of the different groups were similar. The vehicle (DMSO 2%, sterile saline), compounds and indomethacin (100 mM/kg) were orally administered 1 h before the intraplantar (i.pl.) injection of carrageenan (400 mg/20 ml). The paw volume was measured 1, 3 and 5 h after the injection of the inflammatory stimulus. The results are presented as the paw volume (mL) variation in relation to the basal values.

3.11. Evaluation of COX-1 and COX-2 activity and level in vitro and in vivo.

The COX enzyme activity was evaluated using a COX Activity Kit (Enzo Life Science, Farmingdale, NY, USA) according to the instructions. The ovine COX-1, human COX-2 and arachidonic acid not contained in the kit were supplied by Cayman Chemicals and Sigma, respectively. Briefly, test compound or solvent 2.5 μL, assay buffer 35 μL, heme 2.5 μL, and either COX-1 or COX-2 2.5 μL were mixed and incubated for 120 min. Chemiluminescent substrate 10 μL and arachidonic acid 5 μL were added to the re action at room temperature, and immediately read in VICTOR™ X3 multilabel plate reader (PerkinElmer) for 5 s. The peroxidative activity of COX-1 and -2 was determined by a specific chemiluminescent substrate.

The COX-1 and COX-2 enzyme levels was evaluated in mice treated with carrageenan as previously described[71]. Briefly, mice were treated with compound (100 mM/kg, p.o) or vehicle 1 h before carrageenan i.pl. injection. Three hours after carrageenan injection, the rats were anesthetized with chloral hydrate and blood samples were collected from the heart. Blood sample of different groups was centrifuged at 1500 rpm/20 min and the serum was collected and frozen at 70º C. The analysis of COX-1 and COX-2 protein expression was done according to the manufacturer's instruction (for COX-1, USCN Life Science Inc., Houston, TX, USA; for COX-2, R&D Systems, Minneapolis, MN, USA) using a specific antibody coated onto the wells. The plates were then read by a microplate reader at 450 nM.

3.12. AβO preparation.

$A\beta_{1-42}$ peptides (AnaSpec, Fremont, CA, USA) were first dissolved in hexafluoroisopropanol to 1 mg/mL, sonicated, incubated at room temperature for 24 h and lyophilized. The resulting unaggregated $A\beta_{1-42}$ film was dissolved with sterile dimethylsulfoxide to a final concentration of 1 mM and stored at -20°C until use. The $A\beta_{1-42}$ aggregation to oligomeric form was prepared as described previously by Tarozzi et al.[72]. Briefly, $A\beta_{1-42}$ stock in DMSO was diluted into phosphate buffer saline (PBS) at 40 µM and incubated at 4°C for 48 h to enhance oligomer formation[73]. $A\beta_{1-40}$ peptides preparation. Recommended preincubation procedure. $A\beta_{1-40}$ lyophilized peptide was dissolved initially in water to a concentration of 6 mg/ ml. In order to perform the intra-hippocampal injection, it was further diluted with PBS to 800 nmol/ mL and incubated at 37 °C for 4 days.

3.13. Release of pro-inflammatory cytokines IL-1β and TNFα.

Human monocytic THP-1 cells were incubated into 24-well culture plates at 5 x 10^5 cells ml^{-1} with LPS (1 µg/mL) in absence or presence of test compound (10 µM). After 24 h of incubation, THP-1 cells were removed by centrifugation at 500 x *g* for 10 min. The medium was collected and stored at -80°C until further use. The amount of secreted IL-1β and TNFα was assayed using specific ELISA kit High Sensitivity (Thermo Fisher Scientific Inc.) according to the manufacturer's instructions.

3.14. MTT formazan exocytosis induced by AβO.

MTT Formazan Exocytosis induced by AβO was determined using MTT assay, as previously reported[71]. Briefly, SH-SY5Y cells were seeded in 96-well plates at $3x10^4$ cells/well, incubated for 24 h and subsequently treated with compound (20 µM) and AβO (10 µM) for 4 at 37 °C in 5% CO_2. The treatment medium was then replaced with MTT (5 mg/mL) in PBS for 2 h at 37 °C in 5% CO_2. The SH-SY5Y cells were then examined under a microscope and photographed to detect MTT formazan exocytosis. The needle-like crystals on the surface of the cells treated with only AβO, which are easily visible under a light microscope, represent exocytosed MTT formazan.

3.15. Neuronal death induced by AβO.

Neuronal death induced by AβO was determined using the fluorescent probe propidium iodide (PI), as previously reported with minor modification[71]. Briefly, SH-SY5Y cells were seeded in 96-well plates 5 x 10^3 cells/well, incubated for 24 h and subsequently treated with compound (20 µM) and AβO (10 µM) for 24 at 37 °C in 5% CO_2. The treatment medium was then replaced with PI (25 mg/mL) in PBS for 10 min at 37 °C. The stained cells with PI were then examined under a fluorescence microscope. Four randomly selected areas with 50-100 cells in each were analysed and the values obtained are expressed as percentage of dead cells and calculated by the formula: (propidium iodide-positive cells/n total cells) x 100.

3.16. Drug treatment protocol *in vivo*.

All procedures used in this study were approved and strictly followed the ethical principles of animal experimentation adopted by the Ethic Committee on Animal Use of Federal University of Minas Gerais, and institutionally approved under protocol number 336/2012. Experiments were conducted using male C57Bl/6 mice (25–30 g, 10–12 weeks of age) obtained from Animal Care Facilities of the Institute of Biological Sciences (ICB). Animals were kept under controlled room temperature (24 °C) under 12 h: 12 h light-dark cycle, with free access to food and water.

Animals were randomly divided into four major groups (n = 5-8/group) as follows: PBS + vehicle, AβO + vehicle, AβO + test compound. Then, they were anesthetized with an intraperitoneal (i.p.) injection of ketamine (80 mg/kg) and xylazine (8 mg/kg) and then submitted to stereotactic surgery and intrahippocampal injection. The needle was inserted unilaterally and AβO (400 pmol/ 0.5 µ L/mice) or PBS (vehicle) solution was injected into the right hippocampus at the following coordinates from bregma: anteroposterior = −1.9 mm, mediolateral = − 1.5 mm, and dorsoventral = − 2.3 mm. Animals were treated by i.p. administration of 100 mg/ kg of test compound or vehicle 1 hour 30 minutes prior to AβO peptide intra-hippocampal injection and after further 7 days the mice were euthanized and had their brains fixed to evaluate neuronal death and microgliosis using Fluoro-Jade C and Iba-1 staining, respectively.

3.17. Fluoro-Jade C staining.

Fluoro-Jade C (FJC) is an anionic fluorescein derivate used to label degenerating neurons[74]. The hippocampal sections were washed 3 times in PBS for 30 minutes and mounted on gelatinized slides. After drying, slides were immersed in a basic solution of sodium hydroxide (1%) in ethanol (80%) for 5 min, EtOH (70%) for 2 minutes and rinsed with distilled water for 2 minutes. Protected from light, the slides were incubated in a solution of potassium permanganate (0.06%) for 20 minutes, washed with distilled water for 2 minutes and incubated in FJC (Millipore, Billerica, MA, USA) solution (0.0001%) in acetic acid (0.1%) for 20 minutes. Subsequently, they were washed again twice with distilled water for 1 min. After completely drying, slides were dipped in xylene for 1 minute and coverslipped with DPX (Sigma-Aldrich). The slides were observed under fluorescence microscope Zeiss in 10× magnification lens and five different images of the CA1 layer of both hippocampi were taken for quantification of labelled cells using Image J software.

3.18. Iba-1 immunostaining.

The hippocampal section was washed 3 times in Tris-Buffered Saline (TBS) for 30 minutes. Free-floating section were incubated with citrate buffer at 70 °C for 30 minutes, for antigen retrieval. After that, blocking solution [BSA (4%), Triton X (0.5%) in TBS] was added to the section for 2 h, and they were incubated overnight with anti-Iba-1 primary antibody (1:500; Wako Chemicals, Osaka, Japan). On the next day, the section was incubated with the secondary antibody Alexa Fluor 594 anti-rabbit (1:1000; Invitrogen by Thermo Fisher Scientific Inc.) for 1 h, washed, mounted in gelatinized slides and coverslipped with Fluoromount media (Sigma-Aldrich). The slides were observed under a fluorescence microscope in 10× magnification lens and five different images of the CA1 layer of both hippocampi were taken for quantification of labeled cells using Image J software.

3.19. Statistical Analysis

Statistical analysis was performed using the statistical software GraphPad Prism 5.0. In vitro and in vivo data were analysed by one-way ANOVA using an appropriate post-test such as Dunnet, Newman-Keuls or Tukey. The level of significance was set at $p < 0.05$.

4. Conclusions

An increasing number of studies suggest that neuroinflammation significantly contributes to early and late stage of the AD neurodegeneration. In this regard, an anti-inflammatory pharmacological approach could also help to slow the progression or delay the onset of AD. We report the discovery of new multifunctional *N*-benzyl-piperidine-aryl-acylhydrazone derivatives as donepezil hybrids active against both the neuroinflammation and the neurodegenerative processes which occur in AD. Among multifunctional candidate prototypes, compounds **4c** and **4g** showed the best *in silico* ADME parameters, selective inhibition of AChE, anti-inflammatory and neuroprotective properties in several *in vitro* and *in vivo* models. In particular, these compounds recorded the ability to inhibit the release of TNFα from activated microglial cells as well as the activity of COX-1 and COX-2, two pivotal players in the mechanisms of CNS inflammation. Interestingly, inhibition of TNFα by **4c** and **4g** suggest their potential ability to prevent the signal transduction pathway mediated by TNF type 1 receptor (TNFR1) at brain level. It should be noted that TNFR1 are not only involved in AD-related brain neuroinflammation, but also contribute to amyloidogenesis via β-secretase regulation, COX-2 upregulation and activation, synaptic loss, neuronal death and cognitive decline.[75,76] Besides, the data obtained for compounds **4g**, **4c** support these considerations recording the ability to counteract both the microgliosis and the neuronal death induced by unilateral intrahippocampal injection of Aβ in mice. Taking together all these multiple activities related to AD pathogenesis, compound **4c** seems to be the most promising drug prototype candidate for development of genuine multi-target directed drugs for Alzheimer's disease.

Acknowledgements

This work was supported by grants from INCT of Drugs and Medicines (INOFAR, CNPq, Brazil, #573.564/2008-6), FAPEMIG (Brazil, #CEX-APQ-01072-08 #CEX-APQ-01299-10, #CEX-APQ-00807-12, # CEX-PPM-00241-15), Universal and PVE Projects

(CNPq, Brazil, #454088/2014-0, #400271/2014-1), FAPERJ (APQ-1E-26/111.757/2012). The authors are also grateful for the fellowships granted by CAPES, CNPq, FAPEMIG, PIBIC-UFRJ, PIBIC-UNIFAL, PIBICT-UNIFAL and to Prof. Norberto Peporini Lopes and José Carlos Tomás for HRESI-MS analysis and to Prof. Alline Cristina Campos for support in the amyloid beta assays.

References

[1] M.L. Bolognesi, R. Matera, A. Minarini, M. Rosini, C. Melchiorre, Alzheimer's disease: new approaches to drug discovery, Curr. Opin. Chem. Biol. 13 (2009) 303–308. doi:10.1016/j.cbpa.2009.04.619.

[2] M.B.H. Youdim, J.J. Buccafusco, Multi-functional drugs for various CNS targets in the treatment of neurodegenerative disorders, Trends Pharmacol. Sci. 26 (2005) 27–35. doi:10.1016/j.tips.2004.11.007.

[3] Alzheimer Association, 2011 Alzheimer's Disease Facts and Figures, 2011.

[4] A. Agis-Torres, M. Sölhuber, M. Fernandez, J.M. Sanchez-Montero, Multi-Target-Directed Ligands and other Therapeutic Strategies in the Search of a Real Solution for Alzheimer's Disease., Curr. Neuropharmacol. 12 (2014) 2–36. doi:10.2174/1570159X113116660047.

[5] W.J. Geldenhuys, C.J. Van der Schyf, Rationally designed multi-targeted agents against neurodegenerative diseases., Curr. Med. Chem. 20 (2013) 1662–72. doi:10.2174/09298673113209990112.

[6] C.A.M. Fraga, E.J. Barreiro, New Insights for Multifactorial Disease Therapy: The Challenge of the Symbiotic Drugs, Curr. Drug Ther. 3 (2008) 1–13. doi:10.2174/157488508783331225.

[7] H.-Y. Zhang, One-compound-multiple-targets strategy to combat Alzheimer's disease, FEBS Lett. 579 (2005) 5260–5264. doi:10.1016/j.febslet.2005.09.006.

[8] A. Kumar, A. Singh, Ekavali, A review on Alzheimer's disease pathophysiology and its management: an update, Pharmacol. Reports. 67 (2015) 195–203. doi:10.1016/j.pharep.2014.09.004.

[9] M.B.H. Youdim, Why Do We Need Multifunctional Neuroprotective and Neurorestorative Drugs for Parkinson's and Alzheimer's Diseases as Disease

Modifying Agents, Exp. Neurobiol. 19 (2010) 1–14. doi:10.5607/en.2010.19.1.1.

[10] M. Rosini, E. Simoni, M. Bartolini, A. Cavalli, L. Ceccarini, N. Pascu, D.W. McClymont, A. Tarozzi, M.L. Bolognesi, A. Minarini, V. Tumiatti, V. Andrisano, I.R. Mellor, C. Melchiorre, Inhibition of Acetylcholinesterase, β-Amyloid Aggregation, and NMDA Receptors in Alzheimer's Disease: A Promising Direction for the Multi-target-Directed Ligands Gold Rush, J. Med. Chem. 51 (2008) 4381–4384. doi:10.1021/jm800577j.

[11] Alzheimer's Association, 2012 Alzheimer's Disease Facts and Figures, 2012. doi:10.1016/j.jalz.2012.02.001.

[12] B. Ray, D.K. Lahiri, Neuroinflammation in Alzheimer's disease: different molecular targets and potential therapeutic agents including curcumin, Curr. Opin. Pharmacol. 9 (2009) 434–444. doi:10.1016/j.coph.2009.06.012.

[13] F.P.D. Viegas, M.C.R. Simões, M.D. da Rocha, M.R. Castelli, M.S. Moreira, C. V. Junior, Alzheimer's Disease: Characterization, Evolution and Implications of the Neuroinflammatory Process, Rev. Virtual Química. 3 (2011). doi:10.5935/1984-6835.20110034.

[14] B. Schmitt, T. Bernhardt, H.J. Moeller, I. Heuser, L. Frolich, Combination therapy in Alzheimer's disease: A review of current evidence., CNS Drugs. 18 (2004) 827–844.

[15] F.P.D. Viegas, K.S.T. Dias, M.C.R. Simões, M.D. Rocha, M.R. Castelli, M.S. Moreira, C. Viegas Jr., Alzheimer's Disease: Characterization, progress and implications of the neuroinflammatory process., in: Compend. Med. Chem., 1st ed., 2015: p. 388.

[16] H. Akiyama, S. Barger, S. Barnum, B. Bradt, J. Bauer, G.M. Cole, N.R. Cooper, P. Eikelenboom, M. Emmerling, B.L. Fiebich, C.E. Finch, S. Frautschy, W.S.T. Griffin, H. Hampel, M. Hull, G. Landreth, L.F. Lue, R. Mrak, I.R. Mackenzie, P.L. Mcgeer, M.K.O. Banion, J. Pachter, G. Pasinetti, C.P. Salaman, J. Rogers, R. Rydel, Y. Shen, W. Streit, R. Strohmeyer, I. Tooyoma, F.L. Van Muiswinkel, R. Veerhuis, D. Walker, S. Webster, B. Wegrzyniak, G. Wenk, T.W. Coray, Inflammation and Alzheimer ' s disease, Neurobiol. Aging. 21 (2000) 383–421.

[17] A.S.M. Hung, Y. Liang, T.C.H. Chow, H.C. Tang, S.L.Y. Wu, M.S.M. Wai, D.T. Yew, Mutated tau, amyloid and neuroinflammation in Alzheimer disease-A brief

review, Prog. Histochem. Cytochem. 51 (2016) 1–8. doi:10.1016/j.proghi.2016.01.001.

[18] K. Yui, G. Imataka, H. Nakamura, N. Ohara, Y. Naito, Eicosanoids Derived From Arachidonic Acid and Their Family Prostaglandins and Cyclooxygenase in Psychiatric Disorders., Curr. Neuropharmacol. 13 (2015) 776–785. doi:10.2174/1570159X13666151102103305.

[19] H.-L. Hsieh, C.-M. Yang, Role of Redox Signaling in Neuroinflammation and Neurodegenerative Diseases, Biomed Res. Int. (2013) 1–18. doi:10.1155/2013/484613.

[20] Q. Alam, M. Zubair Alam, G. Mushtaq, G. A. Damanhouri, M. Rasool, M. Amjad Kamal, A. Haque, Inflammatory Process in Alzheimer's and Parkinson's Diseases: Central Role of Cytokines, Curr. Pharm. Des. 22 (2016) 541–548. doi:10.2174/1381612822666151125000300.

[21] S.-H. Choi, S. Aid, F. Bosetti, The distinct roles of cyclooxygenase-1 and -2 in neuroinflammation: implications for translational research, Trends Pharmacol. Sci. 30 (2009) 174–181. doi:10.1016/j.tips.2009.01.002.

[22] K.S.T. Dias, C.T. de Paula, M.M. Riquiel, S.T.L. do Lago, K.C.M. Costa, S.M. Vaz, R.P. Machado, L.M.S. de Lima, C. Viegas Jr., Recent Applications of the Multi-Target Directed Ligands Approach for the Treatment of Alzheimer's Disease, Rev. Virtual Química. 7 (2015). doi:10.5935/1984-6835.20150027.

[23] A. Piau, F. Nourhashémi, C. Hein, C. Caillaud, B. Vellas, Progress in the development of new drugs in Alzheimer's disease, J. Nutr. Heal. Aging. 15 (2011) 45–57. doi:10.1007/s12603-011-0012-x.

[24] R. Morphy, C. Kay, Z. Rankovic, From magic bullets to designed multiple ligands, Drug Discov. Today. 9 (2004) 641–651. doi:10.1016/S1359-6446(04)03163-0.

[25] R. Morphy, Z. Rankovic, Designed Multiple Ligands. An Emerging Drug Discovery Paradigm, J. Med. Chem. 48 (2005) 6523–6543. doi:10.1021/jm058225d.

[26] R. León, A.G. Garcia, J. Marco-Contelles, Recent advances in the multitarget-directed ligands approach for the treatment of Alzheimer's disease, Med. Res. Rev. 33 (2013) 139–189. doi:10.1002/med.20248.

[27] J. Jeřábek, E. Uliassi, L. Guidotti, J. Korábečný, O. Soukup, V. Sepsova, M.

Hrabinova, K. Kuča, M. Bartolini, L.E. Peña-Altamira, S. Petralla, B. Monti, M. Roberti, M.L. Bolognesi, Tacrine-resveratrol fused hybrids as multi-target-directed ligands against Alzheimer's disease, Eur. J. Med. Chem. 127 (2017) 250–262. doi:10.1016/j.ejmech.2016.12.048.

[28] D. Panek, A. Więckowska, T. Wichur, M. Bajda, J. Godyń, J. Jończyk, K. Mika, J. Janockova, O. Soukup, D. Knez, J. Korabecny, S. Gobec, B. Malawska, Design, synthesis and biological evaluation of new phthalimide and saccharin derivatives with alicyclic amines targeting cholinesterases, beta-secretase and amyloid beta aggregation, Eur. J. Med. Chem. 125 (2017) 676–695. doi:10.1016/j.ejmech.2016.09.078.

[29] H. Zetterberg, K. Blennow, Plasma Aβ in Alzheimer 's disease — up or down ?, Neurology. 5 (2006) 638–639.

[30] A. Cavalli, M.L. Bolognesi, A. Minarini, M. Rosini, V. Tumiatti, M. Recanatini, C. Melchiorre, Multi-target-directed ligands to combat neurodegenerative diseases, J. Med. Chem. 51 (2008) 347–372. doi:10.1021/jm7009364.

[31] M. Rodrigues Simoes, F. Dias Viegas, M. Moreira, M. Freitas Silva, M. Riquiel, P. da Rosa, M. Castelli, M. dos Santos, M. Soares, C. Viegas, Donepezil: An Important Prototype to the Design of New Drug Candidates for Alzheimer's Disease, Mini-Reviews Med. Chem. 14 (2014) 2–19. doi:10.2174/1389557513666131119201353.

[32] J. Korabecny, R. Dolezal, P. Cabelova, A. Horova, E. Hruba, J. Ricny, L. Sedlacek, E. Nepovimova, K. Spilovska, M. Andrs, K. Musilek, V. Opletalova, V. Sepsova, D. Ripova, K. Kuca, 7-MEOTA–donepezil like compounds as cholinesterase inhibitors: Synthesis, pharmacological evaluation, molecular modeling and QSAR studies, Eur. J. Med. Chem. 82 (2014) 426–438. doi:10.1016/j.ejmech.2014.05.066.

[33] F. Zemek, L. Drtinova, E. Nepovimova, V. Sepsova, J. Korabecny, J. Klimes, K. Kuca, Outcomes of Alzheimer's disease therapy with acetylcholinesterase inhibitors and memantine., Expert Opin. Drug Saf. 13 (2014) 759–774. doi:10.1517/14740338.2014.914168.

[34] A.P. Rodrigues, L.M. Costa, B.L. Santos, R.C. Maia, A.L. Miranda, E.J. Barreiro, C.A. Fraga, Novel furfurylidene N-acylhydrazones derived from natural safrole: discovery of LASSBio-1215, a new potent antiplatelet prototype, J Enzym. Inhib

Med Chem. 27 (2012) 101–109. doi:10.3109/14756366.2011.578575.

[35] C.D. Duarte, E.J. Barreiro, C. a M. Fraga, Privileged structures: a useful concept for the rational design of new lead drug candidates., Mini Rev. Med. Chem. 7 (2007) 1108–1119. doi:10.2174/138955707782331722.

[36] R. Turnaturi, V. Oliveri, G. Vecchio, Biotin-8-hydroxyquinoline conjugates and their metal complexes: Exploring the chemical properties and the antioxidant activity, Polyhedron. 110 (2016) 254–260. doi:10.1016/j.poly.2016.02.025.

[37] G.S. Silva, M. Figueiró, C.F. Tormena, F. Coelho, W.P. Almeida, Effects of novel acylhydrazones derived from 4-quinolone on the acetylcholinesterase activity and A β 42 peptide fibrils formation, J. Enzyme Inhib. Med. Chem. 6366 (2016) 1–7. doi:10.3109/14756366.2016.1144597.

[38] T.R.F. de Melo, R.C. Chelucci, M.E.L. Pires, L.A. Dutra, K.P. Barbieri, P.L. Bosquesi, G.H.G. Trossini, M.C. Chung, J.L. dos Santos, Pharmacological evaluation and preparation of nonsteroidal anti-inflammatory drugs containing an N-acyl hydrazone subunit, Int. J. Mol. Sci. 15 (2014) 5821–5837. doi:10.3390/ijms15045821.

[39] Y.K.C. Da Silva, C.V. Augusto, M.L.D.C. Barbosa, G.M.D.A. Melo, A.C. De Queiroz, T.D.L.M.F. Dias, W.B. Júnior, E.J. Barreiro, L.M. Lima, M.S. Alexandre-Moreira, Synthesis and pharmacological evaluation of pyrazine N-acylhydrazone derivatives designed as novel analgesic and anti-inflammatory drug candidates, Bioorganic Med. Chem. 18 (2010) 5007–5015. doi:10.1016/j.bmc.2010.06.002.

[40] E.J. Barreiro, C. a M. Fraga, A.L.P. Miranda, C.R. Rodrigues, A química medicinal de N-acilidrazonas: Novos compostos-protótipos de fármacos analgésicos, antiinflamatórios e anti-trombóticos, Quim. Nova. 25 (2002) 129–148. doi:10.1590/S0100-40422002000100022.

[41] R.C. Chelucci, L.A. Dutra, M.E.L. Pires, T.R.F. De Melo, P.L. Bosquesi, M.C. Chung, J.L. Dos Santos, Antiplatelet and antithrombotic activities of non-steroidal anti-inflammatory drugs containing an n-Acyl hydrazone subunit, Molecules. 19 (2014) 2089–2099. doi:10.3390/molecules19022089.

[42] G. Rajitha, K.V.S.R.G. Prasad, A. Umamaheswari, D. Pradhan, K. Bharathi, Synthesis, biological evaluation, and molecular docking studies of N-(α-acetamido

cinnamoyl) aryl hydrazone derivatives as antiinflammatory and analgesic agents, Med. Chem. Res. 23 (2014) 5204–5214. doi:10.1007/s00044-014-1091-0.

[43] C.A.M. Fraga, E.J. Barreiro, Medicinal Chemistry of N-Acylhydrazones : New Lead-Compounds of Analgesic , Antiinflammatory and Antithrombotic Drugs, Curr. Med. Chem. 13 (2006) 167–198. doi:10.2174/092986706775197881.

[44] G.L. Ellman, K.D. Courtney, V. Andres Jr., R.M. Featherstone, A new and rapid colorimetric determination of acetylcholinesterase activity, Biochem. Pharmacol. 7 (1961) 88–95.

[45] S. Simon, J. Massoulié, Cloning and Expression of Acetylcholinesterase from Electrophorus, J. Biol. Chem. 272 (1997) 33045–33055.

[46] T. Hashizume, S. Yoshitomi, S. Asahi, R. Uematsu, S. Matsumura, F. Chatani, H. Oda, Advantages of human hepatocyte-derived transformants expressing a series of human cytochrome P450 isoforms for genotoxicity examination, Toxicol. Sci. 116 (2010) 488–497. doi:10.1093/toxsci/kfq154.

[47] I. Valentin-Severin, L. Le Hegarat, J.C. Lhuguenot, A.M. Le Bon, M.C. Chagnon, Use of HepG2 cell line for direct or indirect mutagens screening: Comparative investigation between comet and micronucleus assays, Mutat. Res. - Genet. Toxicol. Environ. Mutagen. 536 (2003) 79–90. doi:10.1016/S1383-5718(03)00031-7.

[48] F. Kassie, W. Parzefall, S. Knasmüller, Single cell gel electrophoresis assay: a new technique for human biomonitoring studies., Mutat. Res. 463 (2000) 13–31. doi:10.1016/S1383-5742(00)00041-7.

[49] M. Fenech, The Cytokinesis-Block Micronucleus Technique and Its Application to Genotoxicity Studies in Human Populations, Environ. Health Perspect. 101 (1993) 101–107. doi:10.1289/ehp.93101s3101.

[50] H. Azizian, Z. Mousavi, H. Faraji, M. Tajik, K. Bagherzadeh, P. Bayat, A. Shafiee, A. Almasirad, Arylhydrazone derivatives of naproxen as new analgesic and anti-inflammatory agents: Design, synthesis and molecular docking studies, J. Mol. Graph. Model. 67 (2016) 127–136. doi:10.1016/j.jmgm.2016.05.009.

[51] K.O. Mohammed, Y.M. Nissan, Synthesis, Molecular Docking, and Biological Evaluation of Some Novel Hydrazones and Pyrazole Derivatives as Anti-inflammatory Agents, Chem. Biol. Drug Des. 84 (2014) 473–488.

doi:10.1111/cbdd.12336.

[52] J.L.M. Tributino, C.D. Duarte, R.S. Corrêa, A.C. Doriguetto, J. Ellena, N.C. Romeiro, N.G. Castro, A.L.P. Miranda, E.J. Barreiro, C.A.M. Fraga, Novel 6-methanesulfonamide-3,4-methylenedioxyphenyl-N-acylhydrazones: Orally effective anti-inflammatory drug candidates, Bioorganic Med. Chem. 17 (2009) 1125–1131. doi:10.1016/j.bmc.2008.12.045.

[53] G. Rimon, R.S. Sidhu, D.A. Lauver, J.Y. Lee, N.P. Sharma, C. Yuan, R.A. Frieler, R.C. Trievel, B.R. Lucchesi, W.L. Smith, Coxibs interfere with the action of aspirin by binding tightly to one monomer of cyclooxygenase-1, Proc. Natl. Acad. Sci. 107 (2010) 28–33. doi:10.1073/pnas.0909765106.

[54] B.J. Orlando, M.G. Malkowski, Crystal structure of rofecoxib bound to human cyclooxygenase-2, Acta Crystallogr. Sect. Struct. Biol. Commun. 72 (2016) 772–776. doi:10.1107/S2053230X16014230.

[55] C.S. De Magalhães, D.M. Almeida, H.J.C. Barbosa, L.E. Dardenne, A dynamic niching genetic algorithm strategy for docking highly flexible ligands, Inf. Sci. (Ny). 289 (2014) 206–224. doi:10.1016/j.ins.2014.08.002.

[56] N. Singh, M. McCoy, R. Tice, E.L. Schneider, A Simple Technique for Quantitation Damage in Individual of Low Levels of DNA Cells, Exp. Cell Res. 175 (1988) 184–191. doi:0014-4827/88 503.00.

[57] R.R. Tice, E. Agurell, D. Anderson, B. Burlinson, a Hartmann, H. Kobayashi, Y. Miyamae, E. Rojas, J.C. Ryu, Y.F. Sasaki, Single Cell Gel / Comet Assay : Guidelines for In Vitro and In Vivo Genetic Toxicology Testing, Environ. Mol. Mutagen. 35 (2000) 206–21. doi:10.1002/(sici)1098-2280(2000)35:3<206::aid-em8>3.0.co;2-j.

[58] D.J. Selkoe, J. Hardy, The amyloid hypothesis of Alzheimer's disease at 25 years., EMBO Mol. Med. 8 (2016) 595–608. doi:10.15252/emmm.201606210.

[59] P. Salahuddin, M.T. Fatima, A.S. Abdelhameed, S. Nusrat, R.H. Khan, Structure of amyloid oligomers and their mechanisms of toxicities: Targeting amyloid oligomers using novel therapeutic approaches, Eur. J. Med. Chem. 114 (2016) 41–58. doi:10.1016/j.ejmech.2016.02.065.

[60] A. Rauk, Why is the amyloid beta peptide of Alzheimer's disease neurotoxic?, Dalt.

Trans. (2008) 1273–1282. doi:10.1039/b718601k.

[61] J. Budni, D.P. Feijó, H. Batista-Silva, M.L. Garcez, F. Mina, T. Belletini-Santos, L.R. Krasilchik, A.P. Luz, G.L. Schiavo, J. Quevedo, Lithium and memantine improve spatial memory impairment and neuroinflammation induced by β-amyloid 1-42 oligomers in rats, Neurobiol. Learn. Mem. 141 (2017) 84–92. doi:10.1016/j.nlm.2017.03.017.

[62] F. Morroni, G. Sita, A. Tarozzi, R. Rimondini, P. Hrelia, Early effects of Aβ1-42 oligomers injection in mice: Involvement of PI3K/Akt/GSK3 and MAPK/ERK1/2 pathways, Behav. Brain Res. 314 (2016) 106–115. doi:10.1016/j.bbr.2016.08.002.

[63] A. Klegeris, P.L. Mcgeer, Toxicity of human monocytic THP-1 cells and microglia toward SH-SY5Y neuroblastoma cells is reduced by inhibitors of 5-lipoxygenase and its activating protein FLAP Abstract : To explore whether the proinflamma-, J. Leukoc. Biol. 73 (2003) 369–378. doi:10.1189/jlb.1002482.Journal.

[64] M.L. Liu, S.T. Hong, Early phase of amyloid beta42-induced cytotoxicity in neuronal cells is associated with vacuole formation and enhancement of exocytosis., Exp. Mol. Med. 37 (2005) 559–66. doi:10.1038/emm.2005.69.

[65] L.F.N. Lemes, G. de Andrade Ramos, A.S. de Oliveira, F.M.R. da Silva, G. de Castro Couto, M. da Silva Boni, M.J.R. Guimarães, I.N.O. Souza, M. Bartolini, V. Andrisano, P.C. do Nascimento Nogueira, E.R. Silveira, G.D. Brand, O. Soukup, J. Korábečný, N.C. Romeiro, N.G. Castro, M.L. Bolognesi, L.A.S. Romeiro, Cardanol-derived AChE inhibitors: Towards the development of dual binding derivatives for Alzheimer's disease, Eur. J. Med. Chem. 108 (2016) 687–700. doi:10.1016/j.ejmech.2015.12.024.

[66] N.G. Castro, R.S. Costa, L.S.B. Pimentel, A. Danuello, N.C. Romeiro, C. Viegas, E.J. Barreiro, C.A.M. Fraga, V.S. Bolzani, M.S. Rocha, CNS-selective noncompetitive cholinesterase inhibitors derived from the natural piperidine alkaloid (-)-spectaline, Eur. J. Pharmacol. 580 (2008) 339–349. doi:10.1016/j.ejphar.2007.11.035.

[67] B.M. Gyori, G. Venkatachalam, P.S. Thiagarajan, D. Hsu, M.V. Clement, OpenComet: An automated tool for comet assay image analysis, Redox Biol. 2 (2014) 457–465. doi:10.1016/j.redox.2013.12.020.

[68] a. T. Natarajan, F. Darroudi, Use of human hepatoma cells for in vitro metabolic activation of chemical mutagens/carcinogens, Mutagenesis. 6 (1991) 399–403. doi:10.1093/mutage/6.5.399.

[69] D.A. Eastmond, J.D. Tucker, Kinetochore localization in micronucleated cytokinesis-blocked Chinese hamster ovary cells a new and rapid assay for identifying aneuploidyinducing agents, Mutat. Res. 224 (1989) 517–525. https://www.google.com.ng/?gfe_rd=cr&ei=6tMKVrO-AZDj8wf65JDgBA#q=D.A.+Eastmond,+J.D.+Tucker,+Kinetochore+localization+in+micronucleated+cytokinesis-blocked+Chinese+hamster+ovary+cells+a+new+and+rapid+assay+for+identifying+aneuploidyinducing+agents,+.

[70] M. Fenech, The in vitro micronucleus technique, Mutat. Res. 455 (2000) 81–95.

[71] K.S.T. Dias, C.T. de Paula, T. dos Santos, I.N.O. Souza, M.S. Boni, M.J.R. Guimarães, F.M.R. da Silva, N.G. Castro, G.A. Neves, C.C. Veloso, M.M. Coelho, I.S.F. de Melo, F.C.V. Giusti, A. Giusti-Paiva, M.L. da Silva, L.E. Dardenne, I.A. Guedes, L. Pruccoli, F. Morroni, A. Tarozzi, C. Viegas, Design, synthesis and evaluation of novel feruloyl-donepezil hybrids as potential multitarget drugs for the treatment of Alzheimer's disease, Eur. J. Med. Chem. 130 (2017) 440–457. doi:10.1016/j.ejmech.2017.02.043.

[72] A. Tarozzi, A. Merlicco, F. Morroni, F. Franco, G. Cantelli-Forti, G. Teti, M. Falconi, P. Hrelia, Cyanidin 3-O-glucopyranoside protects and rescues SH-SY5Y cells against amyloid-beta peptide-induced toxicity., Neuroreport. 19 (2008) 1483–6. doi:10.1097/WNR.0b013e32830fe4b8.

[73] I. Maezawa, H.-S. Hong, R. Liu, C.-Y. Wu, R.H. Cheng, M.-P. Kung, H.F. Kung, K.S. Lam, S. Oddo, F.M. LaFerla, L.-W. Jin, Congo red and thioflavin-T analogs detect Aβ oligomers, J. Neurochem. 104 (2007) 457–468. doi:10.1111/j.1471-4159.2007.04972.x.

[74] P.M.Q. Bellozi, I.V. de A. Lima, J.G. Dória, É.L.M. Vieira, A.C. Campos, E. Candelario-Jalil, H.J. Reis, A.L. Teixeira, F.M. Ribeiro, A.C.P. de Oliveira, Neuroprotective effects of the anticancer drug NVP-BEZ235 (dactolisib) on amyloid-β 1–42 induced neurotoxicity and memory impairment, Sci. Rep. 6 (2016)

1–12. doi:10.1038/srep25226.

[75] R. Medeiros, C.P. Figueiredo, P. Pandolfo, F.S. Duarte, R.D.S. Prediger, G.F. Passos, J.B. Calixto, The role of TNF-α signaling pathway on COX-2 upregulation and cognitive decline induced by β-amyloid peptide, Behav. Brain Res. 209 (2010) 165–173. doi:10.1016/j.bbr.2010.01.040.

[76] X. Cheng, Y. Shen, R. Li, Targeting TNF : a therapeutic strategy for Alzheimer ' s disease, Drug Discov. Today. 19 (2014) 1822–1827. doi:10.1016/j.drudis.2014.06.029.

HIGHLIGHTS

- Novel aryl-acylhydrazone-donepezil hybrids **4c** and **4g** were synthesized as MTDLs.
- Compounds **4c** and **4g** showed IC_{50}= 25.4 and 8.65 μM, respectively for AChE inhibition.
- **4c** and **4g** showed anti-inflammatory activity against AβO-induced neuroinflammation.
- **4c** and **4g** inhibited COX-1/2 and the release of TNF-α in activated microglial cells.
- Compound **4c** seems to be a promising MTDL drug prototype candidate for AD.